Supporting Information

A 3D functional-structural grapevine model that couples the dynamics of water transport with leaf gas exchange

Junqi Zhu[1], Zhanwu Dai[1], Philippe Vivin[1], Gregory A. Gambetta[1], Michael Henke[2], Antony Peccoux[1*], Nathalie Ollat[1], Serge Delrot[1]

1. EGFV, Bordeaux Sciences Agro, INRA, Université de Bordeaux, 33140 Villenave d'Ornon, France
2. Department of Ecoinformatics, Biometrics and Forest Growth, University of Göttingen, 37077 Göttingen, Germany

* Deceased

Author for correspondence: Zhanwu Dai

Email: zhanwu.dai@bordeaux.inra.fr

Tel: +33-(0)5 5757 5922

Fax: +33-(0)5 5757 5003

Table S1 List of parameters used in the model, their values and units

Parameters	description	Values	Unit	Sources
slope_J_{max}	slope for the relationship between Jmax and nitrogen	61.5	umol e^{-1}/ gN/s	Calibration[1]
slope_V_{cmax}	slope for the relationship between Vcmax and nitrogen	38.6	umolCO_2/ gN/s	Calibration
slope_R_d	slope for the relationship between Rd and nitrogen	0.7	umolCO_2/ gN/s	Calibration
slope_$\kappa_{2(LL)}$	slope for the relationship between $\kappa_{2(LL)}$ (photo to electron conversion coefficient) and nitrogen	0.07	umol e^{-1}/ gN/s	Calibration
int_$\kappa_{2(LL)}$	intercept for the relationship between $\kappa_{2(LL)}$ and nitrogen	0.15	umol e^{-1}/ m2/s	Calibration
θ	a convexity factor the value of which was derived through data fitting	0.87	dimen-sionless	Calibration
g_m	Mesophyll conductance for CO_2 diffusion	0.15	mol/m2/ s	Tomàs et al., 2014
leafN_min	minimum amount of leaf nitrogen below which photosynthesis rate is zero	0.17	g/m2	Evers et al., 2010
g_0	Residual stomatal conductance for CO_2 at the light compensation point	0.012	molCO2/ m2/s	Prieto et al., 2012
E_{Vcmax}	E_{Vcmax} is the activation energy for Vcmax	87700	J/mol	Greer & Weedon, 2012
D_{Vcmax}	D_{Jmax} is the deactivation energy for Vcmax	203500	J/mol	Greer & Weedon, 2012
E_{Jmax}	E_{Jmax} is the activation energy for Jmax	63500	J/mol	Greer & Weedon, 2012
D_{Jmax}	D_{Jmax} is the deactivation energy for Jmax	202900	J/mol	Greer & Weedon, 2012
S_j	S_j is an entropy term for both Vcmax and Jmax	650	J/k/mol	Yin & Struik, 2009
K_{mC25}	Michaelis–Menten constant of Rubisco for CO_2	27.238	Pa	Yin & Struik, 2009
E_{KmC}	the activation energy for parameter Kmc	80990	J/mol	Yin & Struik, 2009
K_{mO25}	Michaelis–Menten constant of Rubisco for O_2	16.582	Pa	Yin & Struik, 2009
E_{KmO}	the activation energy for parameter KmO	23720	J/mol	Yin & Struik, 2009
E_{Rd}	the activation energy for parameter Rd	46390	J/mol	Yin & Struik, 2009
Sco25	Relative CO_2/O_2 specificity factor for Rubisco	2.80	kPa/Pa	Yin & Struik, 2009
Esco	activation energy for parameter Sco,	-24460	J/mol	Yin & Struik, 2009
a1	empirical coefficient for the effect of vpd on gs	0.84	dimen-sionless	Yin & Struik, 2009
b1	empirical coefficient for the effect of vpd on gs	0.14	kPa	Yin & Struik, 2009
Parameters for the thermodynamics of water transport				
n	coefficients that characterize a given soil	1.21	Dimen-tionless	Calibration

α_v	coefficients that characterize a given soil	3.21	Dimen-tionless	Calibration
p	coefficients that characterize a given soil	0.50	Dimen-tionless	Tardieu *et al*., 2015
*K*s	soil hydraulic conductivity at saturation	1.00	kg/m/s/pa	Tardieu *et al*., 2015
a	plant's ability to synthesize ABA at a given ψ_{root}	2e-3	umol/s/ Mpa/plant	Calibration
b	scale parameter for the effects of water flux on dilution	2.07	mg/plant/s	Calibration
Amplitude_init	amplitude of the xylem water potential at the start of the simulation	0.40	Dimen-tionless	Tardieu *et al*., 2015
$L_{root,min}$	Minimum value of root conductance	3.20	mg/Mpa/s	Estimation
$L_{root,max}$	maximum value of root conductance	30.00	mg/Mpa/s	Estimation
$\tau_{root,\ transp}{}^2$	coefficient for the effects of transpiration on whole plant root conductance	4.80	1/Mpa	Calibration
$\tau_{root,\ circad}$	coefficient for the effects of circadian on root conductance	0.08	mg/MPa^2/s	Tardieu *et al*., 2015
$\tau_{root,\ ABA}$	coefficient for the effects of ABA on root conductance	0.01	Dimen-tionless	Tardieu *et al*., 2015
$k_{leaf,0}$	leaf conductance under non transpiration condition	0.70	mg/m2/ Mpa/s	Calibration
$k_{leaf,max}$	maximum value of leaf conductance	12.50	mg/m2/ Mpa/s	Estimation
τ_{leaf_transp}	coefficient for the effects of transpiration on leaf conductance	3.00	1/Mpa	Calibration
$\tau_{leaf,\ circad}$	coefficient for the effects of circadian on leaf conductance	0.12	mg/MPa^2/s	Calibration
$\tau_{leaf,\ ABA}$	coefficient for the effects of ABA on leaf conductance	0.01	Dimen-tionless	Tardieu *et al*., 2015
$\tau_{g_s,\ ABA}$	The sensitivity of stomata conductance to ABA	-2.5e-4	m^3/umol	Calibration
$\tau_{g_s,\ \psi_{leaf}}$	The sensitivity of stomata conductance to ψ_{leaf}	-0.4898	1/Mpa	Calibration
δ	coefficient that decribes the rate of the loss of conductivity	6.60	1/Mpa	Hochberg et al., 2016
$\psi_{50\%}$	leaf water potential when 50% of the leaf conductivity is lost	-1.52	Mpa	Hochberg et al., 2016

[1] Calibration is done either fitting the whole model or function to the experimental data, while estimation is based on expert experience or inferred from other data set. The estimated parameters are not critical parameters for the model.

[2] $\tau_{\text{root, transp}}$ is expressed on whole plant root system. In this experiment, our root biomass is approximately 15 g.

Supporting Information Methos S1. Equations for the extended FvCB module.

$$A_{\text{net}} = \min(A_c, A_j) - R_d \qquad \text{(Eq. S1)}$$

$$A_c = \frac{(C_c - \Gamma_*)V_{c,\max}}{C_c + K_{mc}(1 + O/K_{mo})} \quad \text{Rubisco-limited} \qquad \text{(Eq. S2)}$$

$$A_j = \frac{(C_c - \Gamma_*)\,J/4}{C_c + 2\Gamma_*} \quad e^- \text{ transport-limited} \qquad \text{(Eq. S3)}$$

A_{net} is the net photosynthesis rate (µmol CO_2 m^{-2} s^{-1}), A_c is the rubisco-limited photosysnthesis, A_j is the e^- transport-limited photosysnthesis. R_d is the mitochondrial respiration rate in the light (µmol CO_2 m^{-2} s^{-1}), C_c is the CO_2 partial pressure at the chloroplast site (Pa), Γ^* is the CO_2 compensation point (Pa), O is the oxygen partial pressure of the air (Pa), K_{mc} (Pa) and K_{mo} (Pa) are Michaelis–Menten constants of Rubisco for CO_2 and O_2, respectively. $V_{c,\max}$ is the Maximum carboxylation rate, (µmol CO_2 m^{-2} s^{-1}). J is the rate of electron transport, (µmol e^- m^{-2} s^{-1}). The value of C_c depends on A_{net}, and a complex substitution was used to cancel $C_c$in the equation (see Evers *et al.* , 2010).

$$C_c = \frac{\Gamma_* \cdot V_{c,\max} + A_c \cdot K_{mc}(1 + \frac{O}{K_{mo}})}{V_{c,\max} - A_c} \quad \text{Rubisco-limited} \qquad \text{(Eq. S4)}$$

$$C_c = \frac{\Gamma_* \cdot J/4 + A_j \cdot 2\Gamma_*}{J/4 - A_j} \quad e^{-1} \text{ transport-limited} \qquad \text{(Eq. S5)}$$

$$C_i = C_c + A_{net}/g_m \qquad \text{(Eq. S6)}$$

As the stomata resistance used in the transpiration calculation is expressed in physical units (s m^{-1}), not in molar units (m^2 s mol^{-1}), a unit convertion was made:

$$g_{sw} = 1.6 g_s \times \frac{R(T_{leaf} + 273.15)}{P} \qquad \text{(Eq. S7)}$$

g_{sw} is the stomatal conductance to H_2O in crossing the stomata expressed in physical units (m s^{-1}). The value 1.6 is a factor accounting for the faster diffusion of water vapour compared to CO_2 in crossing the stomata. $\frac{R(T_{leaf} + 273.15)}{P}$ is an factor converting the unit of mol m^{-2} s^{-1}

into m s^{-1} based on the ideal gas assumption. R is the universal gas constant (J K^{-1} mol^{-1}). T_{leaf} is the leaf temperature (°C). P is the atmosphere pressure (Pa). Stomatal resistance to water (r_{sw}, s m^{-1}) is the reciprocal of g_{sw}.

Leaf transpiration E (mm s^{-1}) was calculated using the Penman-Monteith equation:

$$E = \frac{sR_n + \frac{\rho c_p VPD_a}{r_{bh} + r_t}}{\lambda(s + \gamma \frac{r_{bw} + r_t + r_{sw}}{r_{bh} + r_t})} \qquad \text{(Eq. S8)}$$

R_n is the net absorbed radiation (photosynthetic active radiation and Near-infrared radiation, in J m^{-2} s^{-1}) calculated by the radiation model; ρc_p is the volumetric heat capacity of air (J m^{-3} K^{-1}, constant); VPD_a is the vapour pressure deficit of the external air (kPa); r_{bh} is the boundary layer resistance to heat (s m^{-1}). r_{bw} is the boundary layer resistance for water (s m^{-1}, taken as 0.96 × r_{bh}); r_t is the turbulence resistance (s m^{-1}); γ is the psychrometric constant (kPa K^{-1}). s is the slope of the curve relating saturation vapour pressure to temperature (kPa K^{-1}), which is affected by leaf temperature.

$$s = \frac{e_{s(T_{leaf})} - e_{s(Ta)}}{T_{leaf} - T_a} \qquad \text{(Eq. S9)}$$

$e_{s(Tleaf)}$ and $e_{s(Ta)}$ are the saturated vapour pressure of the air at the given leaf temperature (T_{leaf}) and air temperature (T_a), respectively (kPa).

Leaf temperature can be calculated from the energy balance between the absorbed radiation, latent heat flux and sensible heat flux.

$$T_{leaf} = T_a + \frac{(r_{bh} + r_t)(R_n - \lambda E_p)}{\rho c_p} \qquad \text{(Eq. S10)}$$

Supporting Information Method S2. Equations for the Tardieu-Davies module.

The Tardieu-Davies model includes a series of calculations: soil water potential as a function of soil water content (Eq. S11); Resistance between rhizosphere and soil-root interface as a function of soil water potential, soil hydraulic conductivity, root radius and mean distance between neighbouring roots (Eqs. S12-S13); Water potential at root surface (hereafter root water potential) as a function of soil water potential, resistance between rhizosphere and soil-root interface and whole plant water flux rate (Eqs. S14-S15); $[ABA]_{xyl}$ as a function of root water potential and water flux (Eq. S16); Water potential inside the root (hereafter xylem water potential) as a function of root water potential, root conductance and plant water flux rate (Eq. S17); Root conductance as a function of water flux rate, $[ABA]_{xyl}$ and circadian oscillation (Eqs. S18-S20); Leaf conductance as a function of water flux rate, $[ABA]_{xyl}$,circadian oscillation (Eqs. S21-S23) and leaf water potential equals to ψ_{xyl} minus the water potential drop caused by leaf transpiration (Eq. S24); Leaf stomata conductance as a function of leaf water potential, $[ABA]_{xyl}$ and maximum stomata conductance at the current ambient condition (Eq. 8, main text).

$$\psi_{soil}(\theta) = \frac{(1-\frac{\theta}{\theta_{sat}})^{(\frac{n}{n-1})^{\frac{1}{n}}}}{(\alpha_v \times \frac{\theta}{\theta_{sat}})^{(\frac{1}{n-1})}} \qquad \text{(Eq. S11)}$$

$$k(\psi_{soil}) = \mathrm{ks}\left(\frac{1}{1+(\alpha_v \times \psi_{soil})^n}\right)^{(p-\frac{p}{n})} \times \left(1-(1-\frac{1}{1+(\alpha_v \times \psi_{soil})^n})^{(1-\frac{1}{n})}\right)^2 \qquad \text{(Eq. S12)}$$

$$R_{sp} = \ln(\frac{d^2}{r^2}) \Big/ 4\pi k(\psi_{soil}) L_a \qquad \text{(Eq. S13)}$$

$\psi_{soil}(\theta)$, MPa, is the soil water potential under current soil water content (θ). $k(\psi_{soil})$, m^2 MPa^{-1} S^{-1}, is the soil hydraulic conductivity at current soil water potential. ks is the soil hydraulic conductivity at saturation. n, α_v, and p are coefficients that characterize a given soil (Table S1). R_{sp} , mg $MPa^{-1}s^{-1}plant^{-1}$ is resistance from rhizosphere to soil–root interface. d, mm, is the mean distance between neighbouring roots. r, mm, is the root radius. L_a, m m^{-2} is the root length per

unit of area. Note L_a is missing in Eq. 6 in Tardieu et al., 2015. An example of the shape of the relationship among soil water content, $\psi_{soil}(\theta)$, $k(\psi_{soil})$ and R_{sp} is presented in Fig. S2.

$$J_{plant} = \sum_{i=1}^{leafNum} E_{leaf,i} \times LeafArea_i \quad \text{(Eq. S14)}$$

$$\psi_{root} = \psi_{soil} - J_{plant} \times R_{sp} \quad \text{(Eq. S15)}$$

$$[ABA]_{xyl} = -a \times \frac{\psi_{root}}{J_{plant} + b} \quad \text{(Eq. S16)}$$

$$\psi_{xylem} = \psi_{root} - \frac{J_{plant}}{L_{root}} \quad \text{(Eq. S17)}$$

J_{plant}, mg $s^{-1}plant^{-1}$, is the whole plant water flux calculated as the sum of leaf transpiration. ψ_{root} is the water potential at root surface (MPa); $[ABA]_{xyl}$ increases linearly with root water potential and is diluted by plant water flux with an offset b (mg s^{-1} $plant^{-1}$). a is the plant's ability to synthesize ABA at a given ψ_{root} (umol s^{-1} MPa^{-1} $plant^{-1}$). L_{root} is the hydraulic conductance of the whole root system (mg $s^{-1}MPa^{-1}plant^{-1}$) calculated via Eqs. S18 to S20.

$$L_{\text{root, transp}} = min\begin{pmatrix} L_{\text{root, 0}} + \tau_{\text{root, transp}} J_{\text{plant}}, \\ L_{\text{root, max}} \end{pmatrix} \quad \text{(Eq. S18)}$$

$$L_{\text{root, circad}} = \tau_{\text{root, circad}} \cos(\text{time}_{\text{photo}} \times \frac{\pi}{12}) \times (\psi_{\text{xyl, max}} - \psi_{\text{xyl, min}}) \quad \text{(Eq. S19)}$$

$$L_{root} = min\begin{pmatrix} \left(L_{\text{root, circad}} + L_{\text{root, transp}}\right) \times \\ \left(1 + \tau_{\text{root, ABA}} \times \ln([ABA]_{\text{xyl}} / 20)\right), \\ L_{\text{root, max}} \end{pmatrix} \quad \text{(Eq. S20)}$$

$L_{\text{root, transp}}$ is the transpiration-dependent fraction of the root hydraulic conductance (mg s^{-1} $MPa^{-1}plant^{-1}$). $\tau_{\text{root, transp}}$ is the sensitivity of $L_{\text{root, transp}}$ to the whole plant water flux. $L_{\text{root, 0}}$ is the minimum root conductance. $L_{\text{root, max}}$ is the maximum root conductance for avoiding unrealistically high conductance. $L_{\text{root, circad}}$ is the circadian-dependent fraction of the root hydraulic conductance. $time_{\text{photo}}$ is time in the photoperiod calculated by the hour of the day minus sunrise time. $\psi_{xyl,\text{max}}$ and $\psi_{xyl,\text{min}}$ are the maximum and minimum ψ_{xyl} in the previous day.

$\tau_{\text{root, circad}}$ (mg MPa^{-2} s^{-1}) is the sensitivity of $L_{\text{root, circad}}$ to the amplitude of ψ_{xyl}. The final L_{root} is calculated as the sum of $L_{\text{root, transp}}$ and $L_{\text{root, circad}}$ times a positive effect of $[ABA]_{\text{xyl}}$ (umol m^{-3}, Eq. S) on leaf conductance. $\tau_{\text{root, ABA}}$ is the sensitivity of L_{root} to the logarithm of $[ABA]_{xyl}$ ($1/\sqrt{m^3 umol^{-1}}$).

$$k_{\text{leaf , } i\text{, transp}} = min\begin{pmatrix} k_{\text{leaf ,0}} + \tau_{\text{leaf, transp}} E_{\text{leaf ,}i}, \\ k_{\text{leaf ,max}} \end{pmatrix} \quad \text{(Eq. S21)}$$

$$k_{\text{leaf , } i\text{, circad}} = cos\left(time_{\text{photo}} \times \pi / 12\right) \times (\psi_{\text{xyl,max}} - \psi_{\text{xyl,min}}) \times \tau_{\text{leaf, circad}} \quad \text{(Eq. S22)}$$

$$k_{\text{leaf ,}i} = min\begin{pmatrix} \left(k_{\text{leaf , } i\text{, circad}} + k_{\text{leaf , } i\text{, transp}}\right) \times \\ \left(1 - \tau_{\text{leaf, ABA}} \times \ln([ABA]_{\text{xyl}} / 20)\right) \times (1 - f_{\text{PLC}}), \\ k_{\text{leaf ,max}} \end{pmatrix} \quad \text{(Eq. S23)}$$

$k_{\text{leaf , } i\text{, transp}}$ is the transpiration-dependent fraction of the leaf hydraulic conductance (mg m^{-2} s^{-1} MPa^{-1}). It increases linearly with the leaf transpiration rate ($E_{\text{leaf ,}i}$, mg m^{-2}s^{-1}). $\tau_{\text{leaf\_transp}}$ is the sensitivity of $k_{\text{leaf ,}i\_\text{transp}}$ to the leaf transpiration rate (MPa^{-1}). $k_{\text{leaf ,0}}$ is the leaf conductance under non transpiration condition. $k_{\text{leaf ,max}}$ is the maximal leaf conductance for avoiding unrealistically high conductance at high transpiration. $k_{\text{leaf , } i\text{, circad}}$ which is the circadian-dependent fraction of the hydraulic conductance, peaks early in the morning, then decreases and reaches the lowest value when $time_{\text{photo}}$ equals to 12. $time_{\text{photo}}$ is time in the photoperiod calculated as the hour of the day minus sunrise time. $\psi_{\text{xyl, max}}$ and $\psi_{\text{xyl, min}}$ are the maximal and minimal ψ_{xyl} in the previous day. $\tau_{\text{leaf, circad}}$ (mg MPa^{-2} s^{-1}) is the sensitivity of $k_{\text{leaf , } i\text{, circad}}$ to the amplitude of ψ_{xyl}. The final $k_{\text{leaf ,}i}$ is calculated as the sum of $k_{\text{leaf , } i\text{, circad}}$ and $k_{\text{leaf , } i\text{, transp}}$ times a negative effect of $[ABA]_{\text{xyl}}$ (umol m^{-3}) (Pantin *et al.*, 2013; Tardieu *et al.*, 2015) and a negative effect of f_{PLC} on leaf conductance (Hochberg *et al.*, 2016). Note that as no quantitative

relationship between f_{PLC} and water potential was found on root, the effect of f_{PLC} was not included in the calculation of root conductance. $\tau_{\mathrm{leaf,\ ABA}}$ is the sensitivity of $k_{\mathrm{leaf},i}$ to the logarithm of $[ABA]_{\mathrm{xyl}}$ ($1/\sqrt{\mathrm{m^3 umol^{-1}}}$).

$$\psi_{\mathrm{leaf},i} = \psi_{\mathrm{xyl}} - \frac{E_{\mathrm{leaf},i}}{k_{\mathrm{leaf},i}} \qquad \text{(Eq. 24)}$$

Leaf water potential equals to ψ_{xyl} minus the water potential drop caused by leaf transpiration. Combining Eq. S24 with Eq. S21, the value of $\tau_{\mathrm{leaf,\ transp}}$ can be estimated as the reciprocal of the water potential difference between ψ_{xyl} and ψ_{leaf}. The data for midday ψ_{xyl} and ψ_{leaf} were derived from Williams & Araujo, (2002) measured on *Vitis vinifera* L. cv. Cabernet Sauvignon.

Hochberg U, Albuquerque C, Rachmilevitch S, Cochard H, David-Schwartz R, Brodersen CR, McElrone A, Windt CW. **2016**. Grapevine petioles are more sensitive to drought induced embolism than stems: evidence from in vivo MRI and microCT observations of hydraulic vulnerability segmentation. *Plant, Cell & Environment*: 1–9.

Pantin F, Monnet F, Jannaud D, Costa JM, Renaud J, Muller B, Simonneau T, Genty B. **2013**. The dual effect of abscisic acid on stomata. *New Phytologist* **197**: 65–72.

Tardieu F, Simonneau T, Parent B. **2015**. Modelling the coordination of the controls of stomatal aperture, transpiration, leaf growth, and abscisic acid: update and extension of the Tardieu–Davies model. *Journal of Experimental Botany* **66**: 2227–2237.

Williams LE, Araujo FJ. **2002**. Correlations among predawn leaf, midday leaf, and midday stem water potential and their correlations with other measures of soil and plant water status in Vitis vinifera. *Journal of the American Society for Horticultural Science* **127**: 448–454.

Supporting Information Method S3. Leaf gas exchange determination.

Ten leaves with similar physiological age (LPI 10 ± 2) were chosen for the measurements. All measurements were done at a saturating PPFD of 2000 μmol m^{-2} s^{-1}, ambient CO_2 concentration (C_a) of 380 μmol mol^{-1}, relative humidity of 60% and air temperature of 25 °C with a resulting leaf temperature of approximately 27 °C. The air flow fed through the chamber was controlled at 750 mL min^{-1}. Each leaf sample was allowed to adapt to the cuvette conditions for 2 min and was recorded when stable values were observed by the real-time monitoring panel.

Light response curves were established on three well-watered plants using leaves with similar physiological age (LPI 10 ± 2). The cuvette microclimate was set as described above while the PPFD were decreased stepwise: 1500, 1250, 1000, 750, 500, 350, 250, 200, 150, 100, 60, 40, 20 and 0 μmol m-2 s-1. Before recording the gas exchange values at each PPFD, leaves were allowed to adapt to the new condition for 10 minutes.

Supporting Information Methods S4. Equations for theorectial framework for describing the plant responses to drying soil as developed by Martinez-Vilalta et al. (2014):

Under steady-state conditions, water transport through the xylem must balance transpiration losses from leaves.

$$J_{\text{plant}} = g_{\text{leaf}} \times A_{\text{leaf}} \times VPD = -k_{\text{sap}} \times A_{\text{sap}} \times (\psi_{\text{leaf}} - \psi_{\text{soil}}) \qquad \text{(Eq. S25)}$$

$$\psi_{\text{leaf}} - \psi_{\text{soil}} = -\frac{J_{\text{plant}}}{k_{\text{sap}} \times A_{\text{sap}}} = -\frac{A_{\text{leaf}} \times VPD \times g_{\text{leaf}}}{A_{\text{sap}} \times k_{\text{sap}}} \qquad \text{(Eq. S26)}$$

g_{leaf}, leaf conductance for water vapour; k_{sap}, whole-plant hydraulic conductance per unit of basal sapwood cross-sectional area; A_{leaf} is the plant leaf area, while A_{sap} is basal sapwood area. As soil drought develops (i.e. ψ_{soil} declines, becoming more negative), k_{sap} is likely to decline because of the occurrence of xylem embolism (among other processes) and g_{leaf} will be reduced by stomatal closure. An overall response of k_{sap} and g_{leaf} to ψ_{soil} ($f_k(\psi_{\text{soil}})$ and $f_g(\psi_{\text{soil}})$, respectively) was define.

$$\begin{aligned} \psi_{\text{leaf}} &= \psi_{\text{soil}} - \frac{A_{\text{leaf}} \times VPD \times g_{\text{leaf,max}} \times f_g(\psi_{\text{soil}})}{A_{\text{sap}} \times k_{\text{sap,max}} \times f_k(\psi_{\text{soil}})} \\ &= \psi_{\text{soil}} + \Lambda \times \frac{f_g(\psi_{\text{soil}})}{f_k(\psi_{\text{soil}})} = \psi_{\text{soil}} + \Lambda \times \Theta(\psi_{\text{soil}}) \end{aligned} \qquad \text{(Eq. S27)}$$

Λ, measure of the (maximum) transpiration rate per unit of water transport capacity or, equivalently, the leaf water potential at $\psi_{\text{soil}} \approx 0$ (the pressure drop or 'pulling' capacity of the plant when there is plenty of water available in the soil).

It should be noted that, when $\psi_{\text{soil}} \approx 0$, by definition $f_g = f_k = 1$, so that Λ is the intercept of the relationship in Eq S27. Interestingly, if Λ is assumed to be relatively constant, at the temporal scales of interest, compared with g_{leaf} and k_{sap}, it follows that the relative sensitivity of stomata and plant hydraulic conductance to declining soil water potentials (f_g / f_k) determines whether the water potential gradient in the plant declines, increases or stays approximately constant as drought progresses. In more general terms (i.e. without making any assumptions on how or where water transport is regulated), Eqs. S26 and S27 imply that the pressure drop in the plant will increase if the hydraulic conductance declines more rapidly than

the transpiration rate as drought progresses, whereas it will be reduced if the transpiration rate declines more rapidly than the plant hydraulic conductance.

If it is assumed that the Θ function in Eq. S27 is approximately linear within biologically reasonable ranges of water potentials, the relationship between ψ_{leaf} and ψ_{soil} also becomes a linear function, and its slope (σ) determines the magnitude of the reduction in ψ_{leaf} and ψ_{soil} declines (see the Supporting Information of Martinez-Vilalta et al. (2014)):

$$\begin{aligned}\psi_{leaf} &= \psi_{soil} + \Lambda \times \Theta(\psi_{soil}) \approx \Lambda + (1 + \Lambda \times c_{gk}) \times \psi_{soil} \\ &= \Lambda + \sigma \times \psi_{soil}\end{aligned} \qquad \text{(Eq. S28)}$$

In this equation, the value of σ determines the behaviour of plants according to the classical iso/anisohydry paradigm. σ = 0 implies strict isohydry (constant ψ_{leaf} as ψ_{soil} declines), whereas σ = 1 implies strict anisohydry (the difference between ψ_{leaf} and ψ_{soil} stays constant). It should be noted that two other behaviours are possible: for σ > 1, there is extreme anisohydry, implying an increase in the pressure drop through the plant as ψ_{soil} declines, whereas 0 < σ < 1 implies a sort of partial isohydric, by which the difference between ψ_{leaf} and ψ_{soil} is reduced as ψ_{soil} declines.

Supporting Information Methods S5 the sensitivity of model performance to Ta, CO_2, ψ_{soil} and their interactions

To assess the model performance under various environmental conditions, a sensitivity analysis was conducted to test the responses of stomatal conductance, net photosynthesis, and plant water flux to T_a, CO_2, soil water potential (ψ_{soil}) and their interactions. T_a was varied from 13 to 40°C with an interval of 3°C. CO_2 was varied from 100 to 1000 ppm with an interval of 100 ppm. ψ_{soil} was varied from -1.5 to 0 MPa with an interval of 0.1667 MPa. Two by two combinations of those three variables were first simulated and then a full combination of the three variables was also tested. When one variable is not under test, a default value is used. The default value of T_a is 25 ^oC, CO_2 is 400 ppm, ψ_{soil} is -0.3 MPa, R_a is 2000 umol $m^{-2}s^{-1}$ (PAR is 1100 umol $m^{-2}s^{-1}$), *VPD* is 1 kPa. Since air temperature determines the maximal *VPD*, the effects of *VPD* were simulated separately. The result section only presents the stomatal conductance for water (g_{sw}).

The response of stomatal conductance to T_a, CO_2 and ψ_{soil}

Response to single factors Stomatal conductance increased by approximately one fold when air temperature increased from 13 ^oC to 31 ^oC, and then decreased with an accelerating speed especially when temperature is beyond 35 ^oC (Fig. S7a). The reduction in A_{net} was more pronounced than g_{sw} at high temperature (Fig. S8a). A_{net} decreased by approximately three fold when T_a increases from 28 ^oC to 40 ^oC. Water flux increased linearly from 13 ^oC to 37 ^oC and then drops at 40 ^oC (Fig. S9a).

Stomatal conductance and water flux decreased by three fold when CO_2 concentration increased from 100 ppm to 1000 ppm (Fig. S7e, and Fig. S9e), while A_{net} increased by about five fold (Fig. S8e). Stomatal conductance, water flux and A_{net} all decreased exponentially with decreasing soil water potential (Fig. S7i), and close to zero when soil water potential was less than -1.0 MPa.

Response to factors in interactions Larger variability in stomatal conductance across difference temperatures were simulated at low CO_2 concentration than at high CO_2 concentration (T_a × CO_2, Fig. S7d). On average the stomatal conductance under different temperatures at 400 ppm of CO_2 is twice as large as that at 1000 ppm of CO_2. The effects of temperature and CO_2

concentration on stomatal conductance gradually diminished when soil water potential become more negative ($T_a \times \psi_{soil}$, $CO_2 \times \psi_{soil}$, Fig. S7 c, h). The combination of the lowest CO_2 concentration (100 ppm) and highest soil water potential (0 MPa) showing the highest stomatal conductance in all the simulations (Fig. S7 f, h).

In addition, stomatal conductance decreased exponentially with the increasing *VPD* (Supporting Information Fig. S10). However, the simulated water flux increased with growing *VPD* under low temperature and radiation, but decreased with growing *VPD* under high temperature and radiation.

Supporting Information Methods S6 set up of the model simulation

All simulations were made with infinite canopies, although only nine plants were described explicitly in a computer. The infinite canopy was formed by virtual replications which simulates a periodic canopy from a finite set of plants. The nine plants were configured in three rows with three plants in each row. Row distance was set to 0.8 meter, and plant distance was set to 0.3 meter based on the row settings in the greenhouse. The mean of the nine plants was used in the calculation and optimization.

The summed leaf area of a single plant during the simulation was 0.12 m^2 (18 leaves per plant). For facilitating the comparison between simulation and observation results during calibration and validation, the unit of the observed hourly plant water flux was first converted into milligram per unit of square meter and then converted back into plant level based on the leaf area of the simulated plant.

Same simulation configurations were used for the sensitivity analysis with three exceptions for cancelling the carry over effects of one step on the following steps, namely: 1). f_{PLC} was calculated based on ψ_{xyl} as there is no previous ψ_{leaf} ; 2). g_0 was reset to the default value at the end of each step; 3). circadian effects on root and leaf conductance was cancelled by setting the hour of day to 12.

Supporting Information figures:

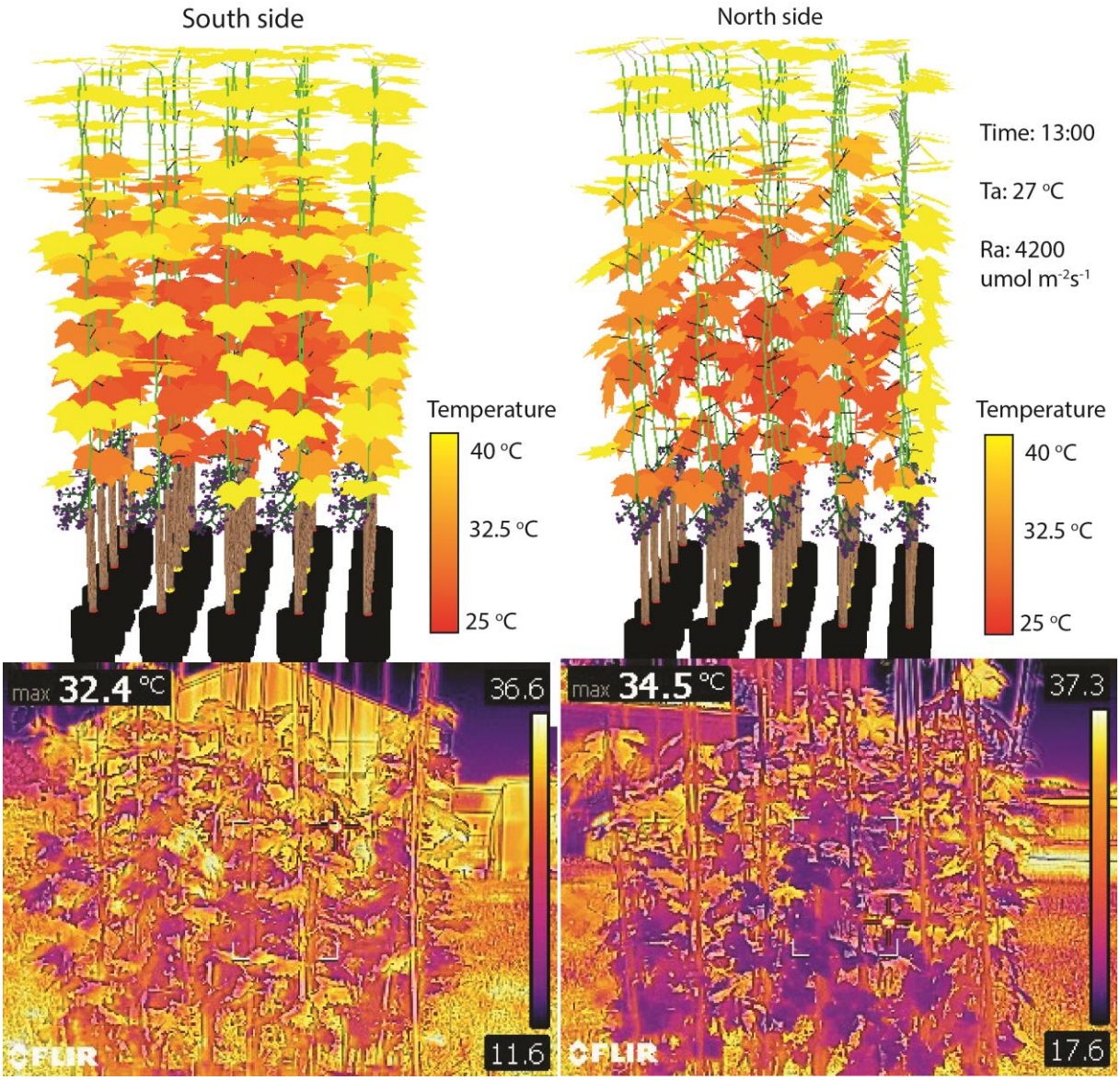

Fig. S1 Comparison of the simulated canopy leaf temperature and canopy thermal picture. Thermal pictures were taken on a sunny and cloudless day with weak wind speed by a FLIR thermal camera (FLIR T450sc FLIR Systems AB, Frankfurt am Main, Germany). Plants in greenhouse were moved to open field, and arranged into a small square (5 rows with 5 plants per row). Row distance and plant distance were both 0.15 meter. Simulations were made with the same plant arrangement. Both direct radiation and diffuse radiation were included in the simulation. The position of the direct radiation was calculated by the latitude, day of year, and time of the day.

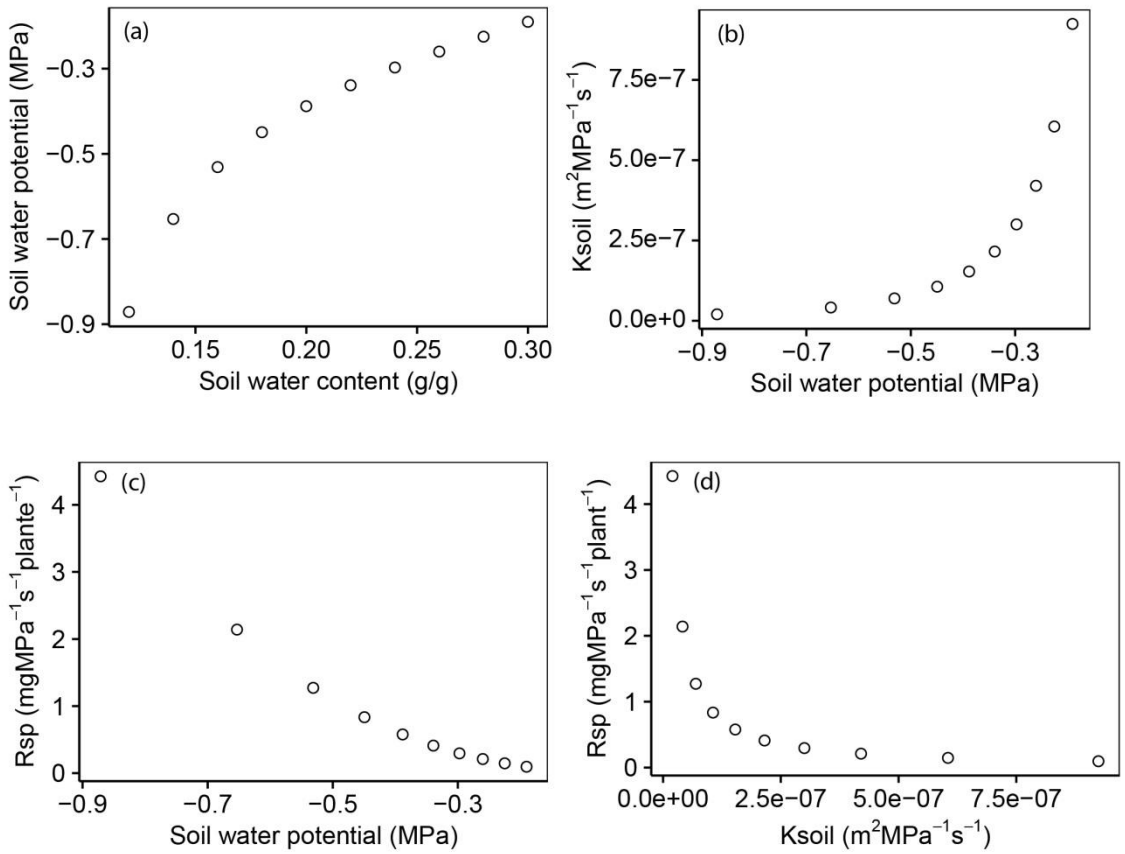

Fig. S2 Relationship between soil water potential and soil water content (a), soil hydraulic conductivity ($k(\psi_{soil})$) and soil water potential (b), the resistance from soil to root surface (R_{sp}) and soil water potential (c), and the resistance from soil to root surface and soil hydraulic conductivity (d). The saturated soil water content in this experiment was 0.352 kg/kg, and wilting soil water content was 0.086 kg/kg.

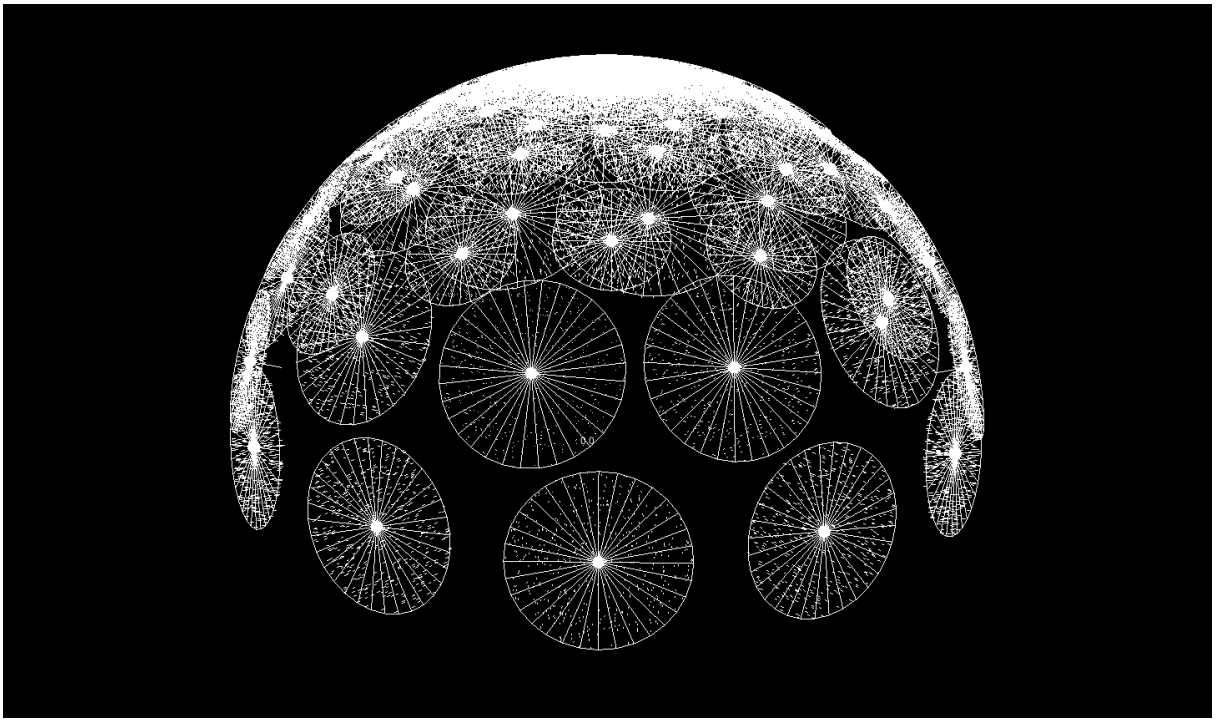

Fig. S3 Illustration of the arrangement of diffuse radiation in a virtual hemisphere. Diffuse radiation was approximated using an array of 72 directional surface light sources positioned regularly in a hemisphere in six circles with 12 light sources each. The partitioning of the total radiation intensity over the 72 diffuse light sources was based on the location of each light source in the sky with top light sources have high proportions. The surface area of each light source equals to the field size.

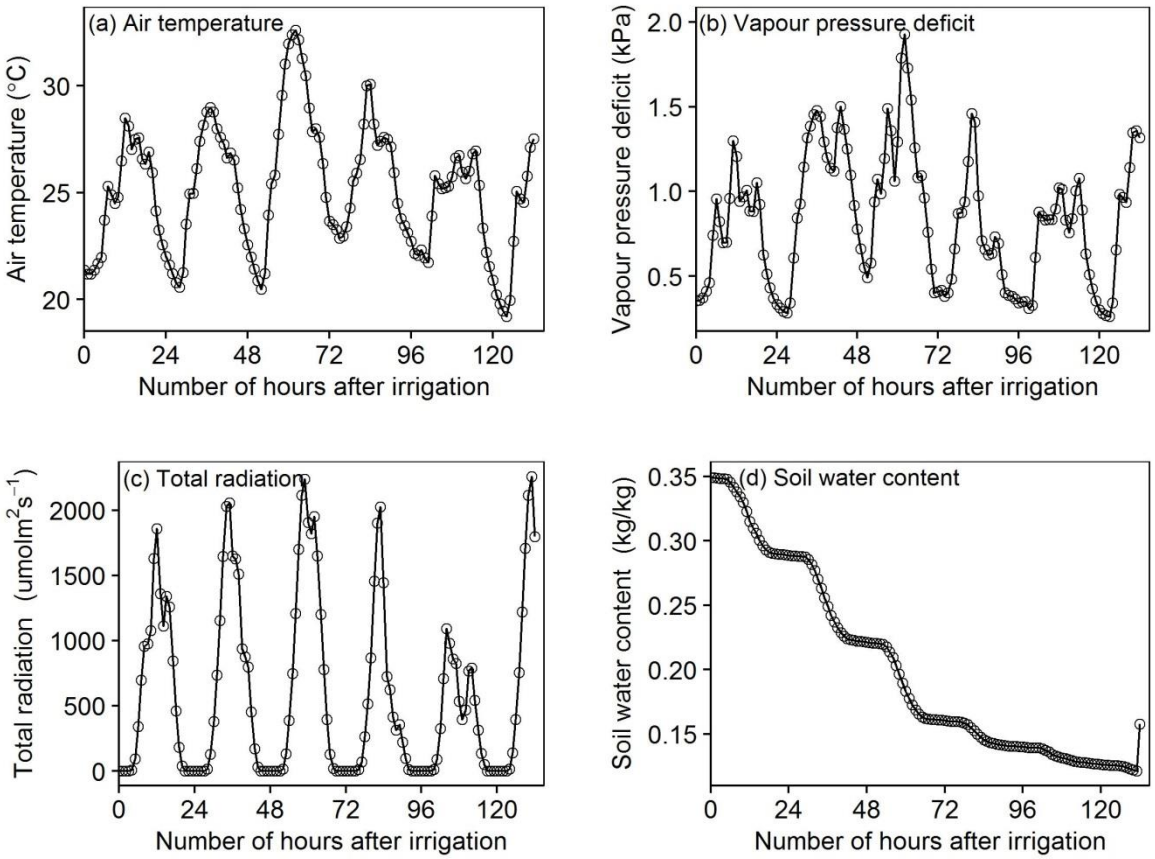

Fig. S4 Hourly mean air temperature (a), vapour pressure deficit (b), total radiation (c) and soil water content (d) recorded during the drying cycle. One week before the beginning of the drying cycle, the plants were irrigated to 100% of soil water holding capacity (0.35 ± 0.04 kg H_2O/kg soil) every day. The irrigation was then stopped for six days. A new irrigation were made on day 6 around 13 o'olock (134 hours after the irrigation counted from zero o'olock the day after stopping irrigation). Circles represent the mean of each hour, and lines is the trajectary of the circles.

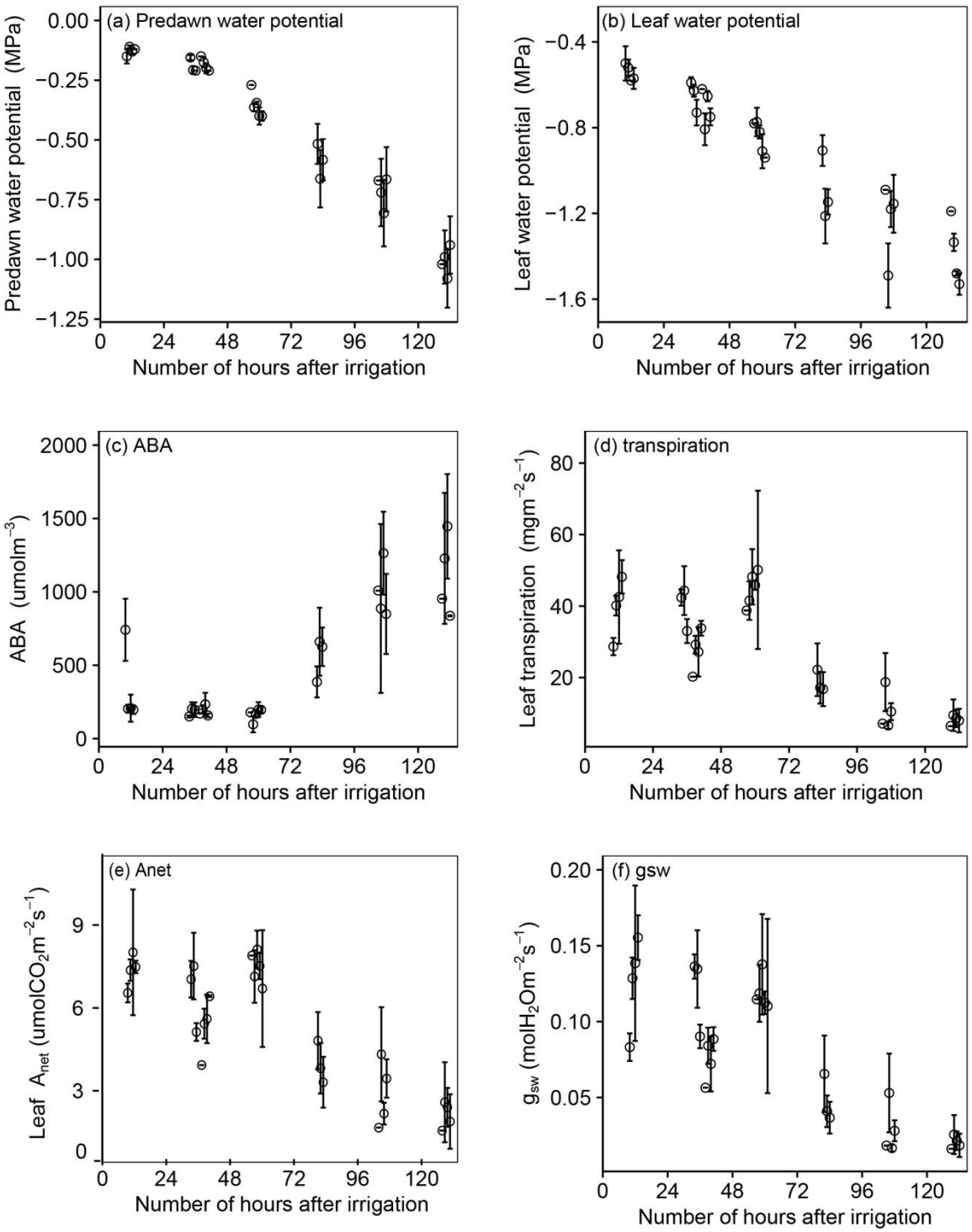

Fig. S5 Predwan soil water water potential (a), leaf water potential (close to midday, b), xylem sap ABA concentration (c), leaf transpiration rate (d), leaf net photosynthesis (e), stomata conductance for water (f) measured during the drying cycle. Measurements were done between 10:00 and 13:00 except few points. Circles represent the mean of each hour. Error bars represent one standard error (mean± se).

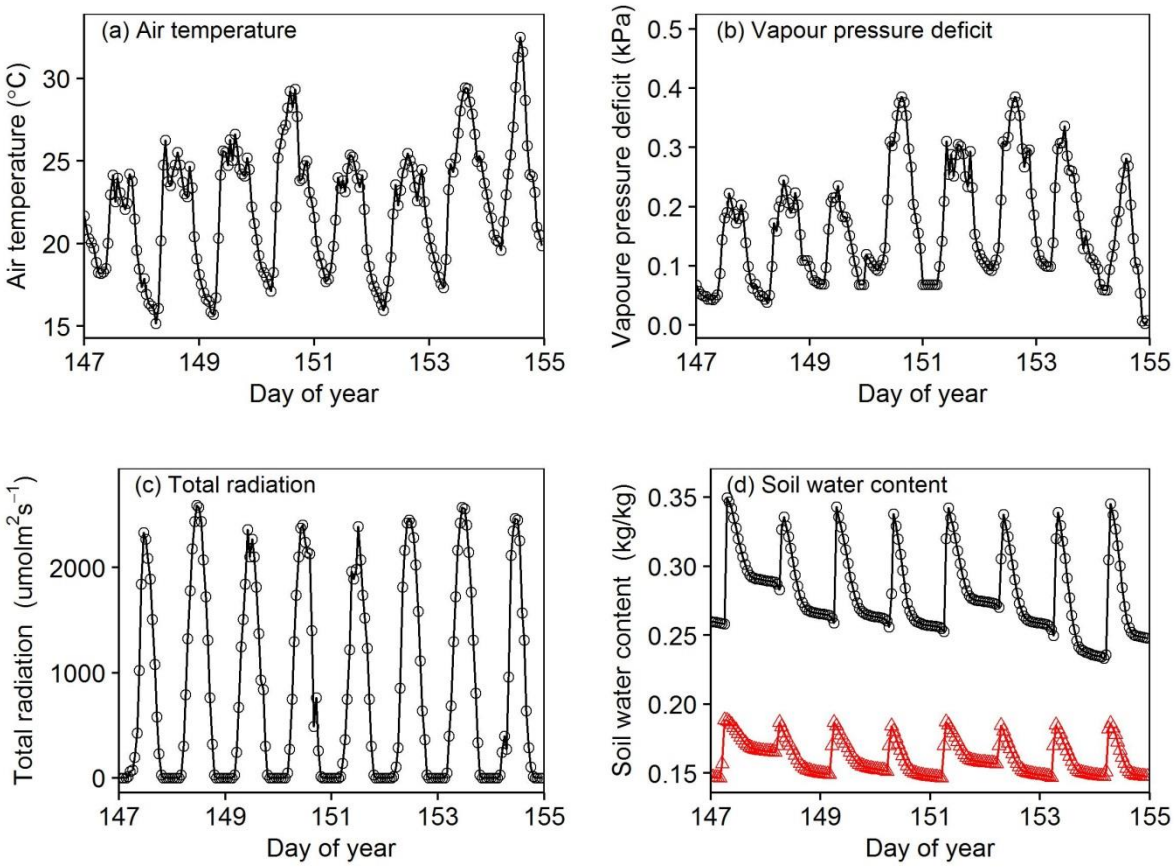

Fig. S6 Hourly mean air temperature (a), vapour pressure (b), total radiation (c) and soil water content (d) of the model validation data set. Black circles in the panel (d) represent the soil water content under the well-watered condition, and red triangles represent the soil water content under the water-stressed condition.

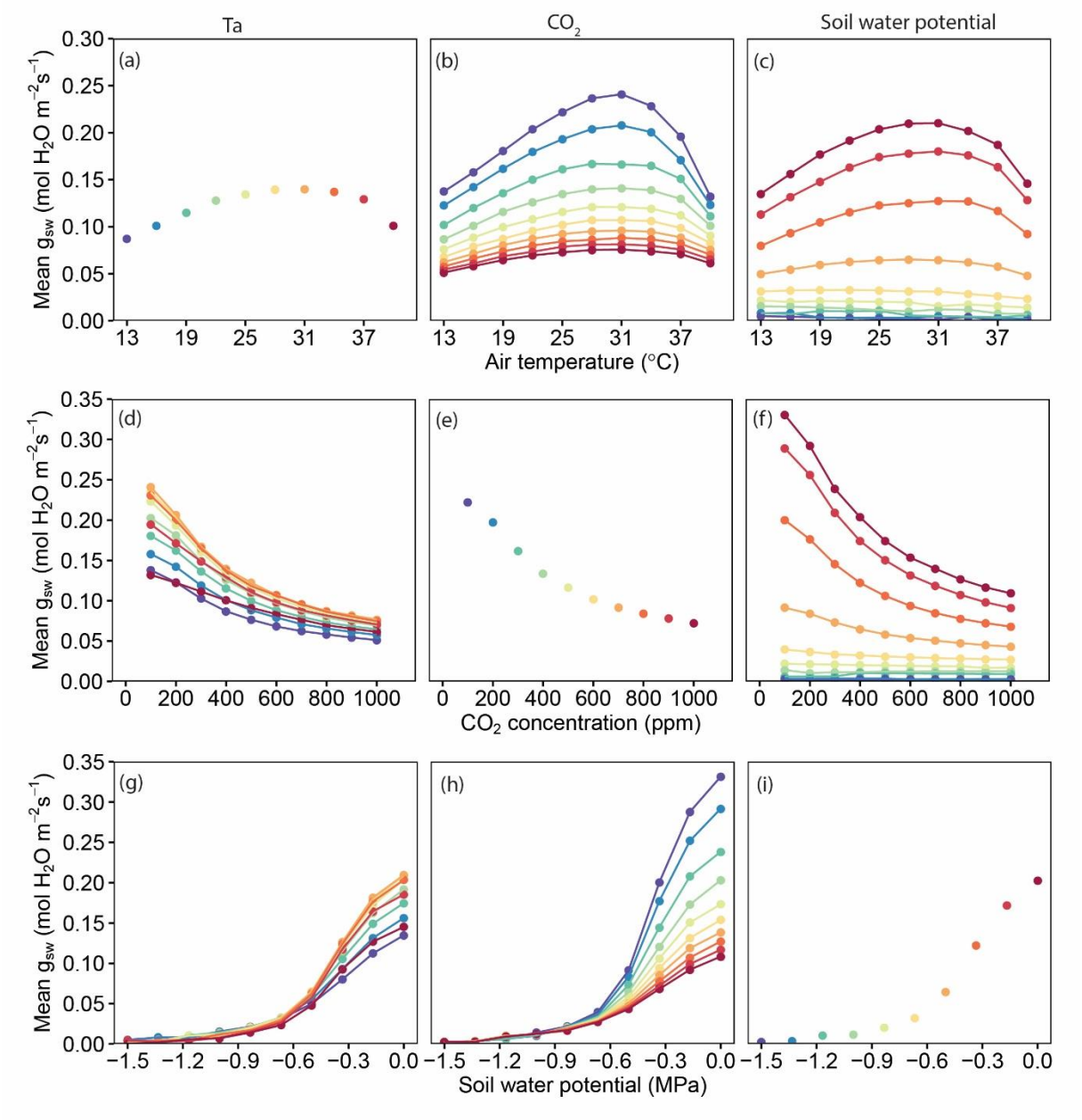

Fig. S7. Response of stomatal conductance to changes in temperature, CO_2 and soil water potential. The figure is presented as an orthogonal square. The colours in column 1 represent different temperatures as indicated in panel (a). The colours in column 2 represent different CO_2 as indicated in panel (e). The colours in column 3 represent different soil water potentials as indicated in panel (i). Note leaf temperature is approximately 3-5 ^{o}C higher than air temperature depending on the absorbed radiation and transpiration rate. The presented g_{sw} is the mean g_{sw} of all leaves of a plant.

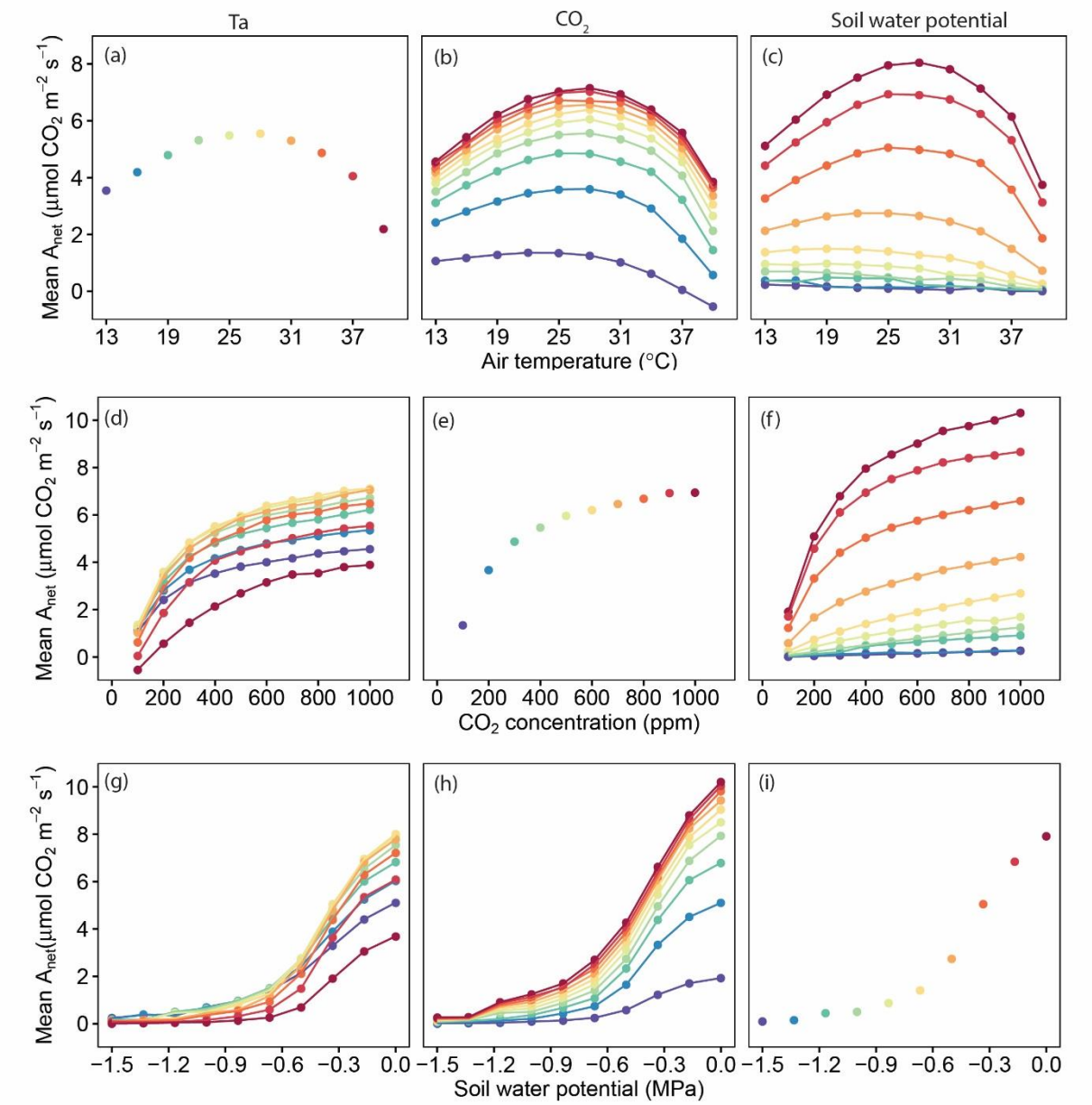

Fig. S8 The response of net photosynthesis to changes in temperature (column one and row one), CO_2 (column two and row two), and soil water potential (column three and row three). The figure is presented as an orthogonal square. The colours in column one represent different temperature as indicated in panel (a). The colours in column two represent different CO_2 as indicated in panel (e). The colours in column three represent different soil water potentials as indicated in panel (i). Note leaf temperature is approximately 3-5 ^{o}C higher than air temperature depending on the absorbed radiation and transpiration rate. The presented A_{net} is the mean A_{net} of all leaves of a plant.

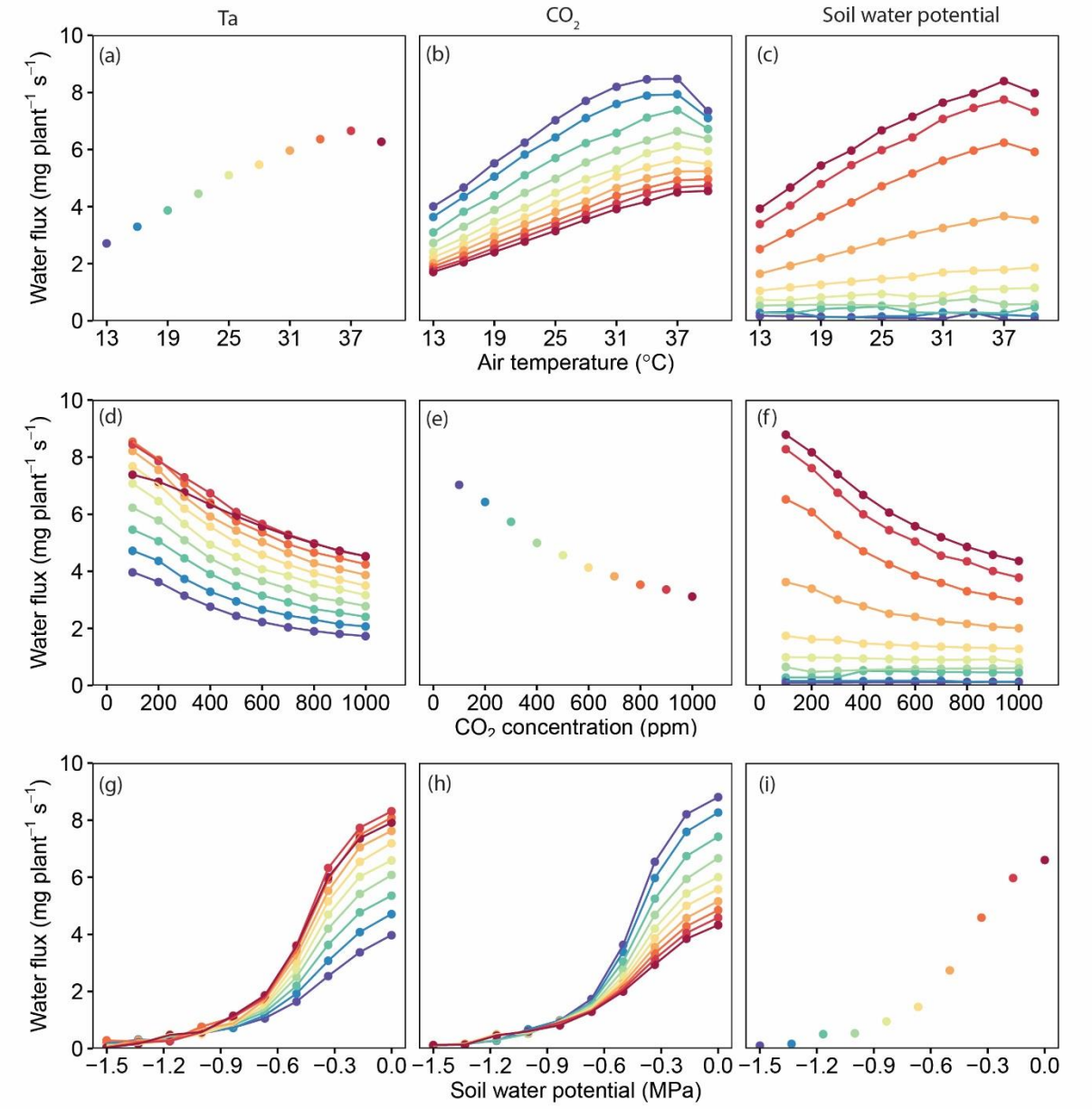

Fig. S9 The response of plant water flux to changes in temperature (column one and row one), CO_2 (column two and row two), and soil water potential (column three and row three). The colours in column one represent different temperature as indicated in panel (a). The colours in column two represent different CO_2 as indicated in panel (e). The colours in column three represent different soil water potentials as indicated in panel (i). Note leaf temperature is approximately 3-5 ^{o}C higher than air temperature depending on the absorbed radiation and transpiration rate.

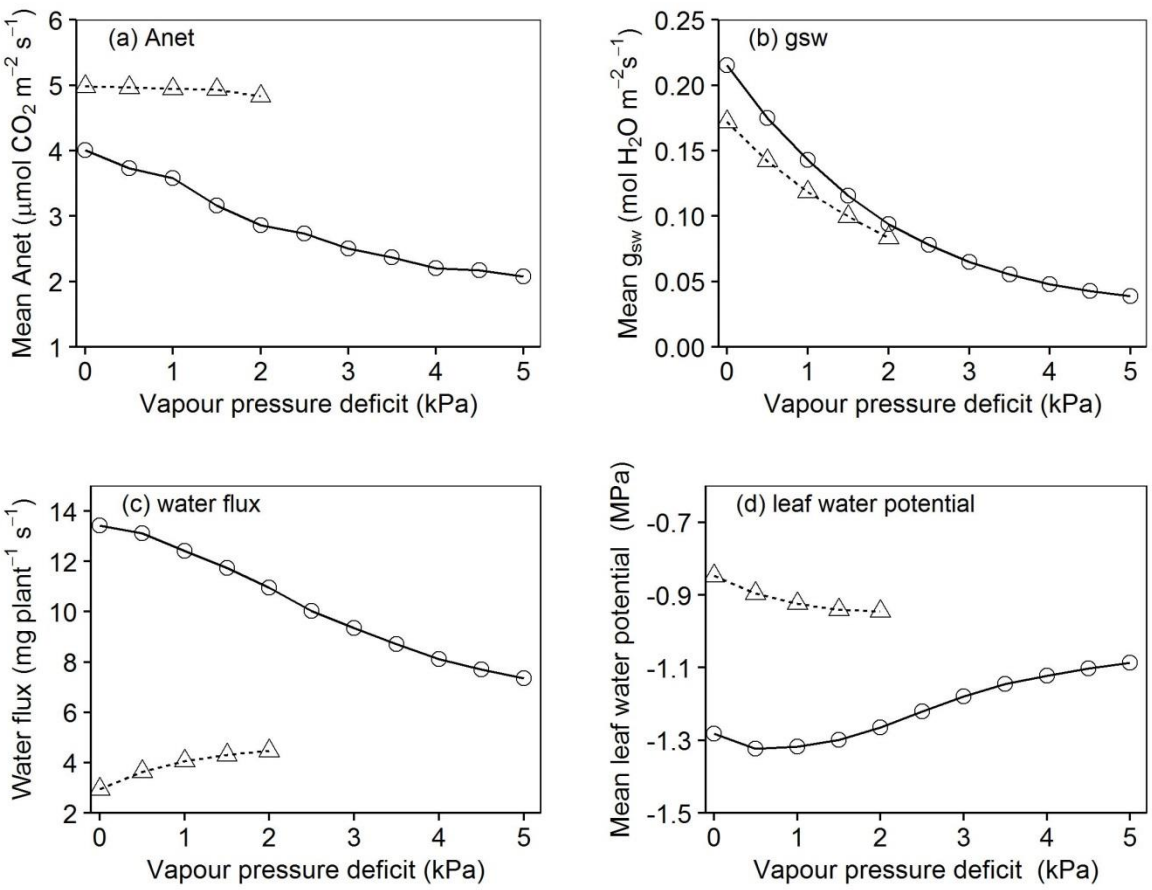

Fig. S10 The response of net photosynthesis (a), stomata conductance for water (b), whole plant water flux (c) and leaf water potential (d) to changes in vapour pressure deficit. Open circles and solid lines were simulations with high air temperature and high radiation (T_a equals to 35 ^oC and R_a equals to 4000 umol $m^{-2}s^{-1}$). Open triangles and dashed lines were simulations with low air temperature and radiation (T_a equals to 20 ^oC and R_a equals to 2000 umol $m^{-2}s^{-1}$). CO_2 was set to 400 ppm and ψ_{soil} was set to -0.3 MPa at both simulation scenarios. All simulations were made with nine plants, and only the middle plants were used in the calculation.

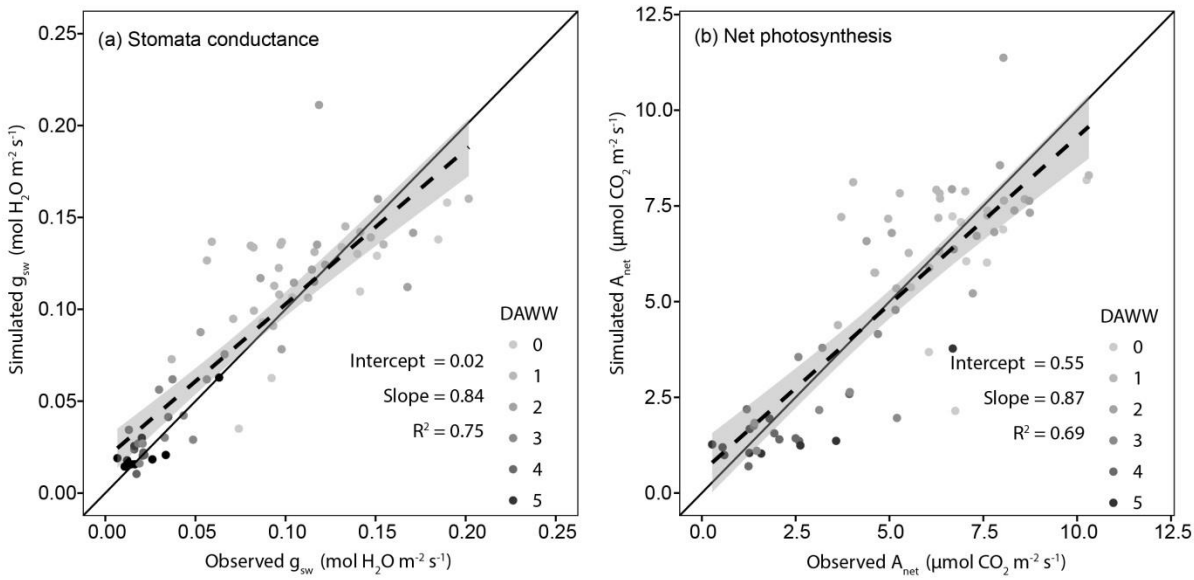

Fig. S11 Verification of the stomata conductance calculated from $[ABA]_{xyl}$ and ψ_{leaf} (Eq. 7, panel a), and verification of the net photosynthesis calculated by the extended-FvCB model with the stomata conductance calculated in panel a as input (panel b). Points are observed values determined on individual leaves within the drying cycle experiment. Solid lines represent the 1:1 relationship between observed and simulated values. Dashed lines are linear regression line between simulated and observed values. Shaded areas around the dashed lines are the 95% confidence interval of the fitted values. DAWW represents days after withholding water.

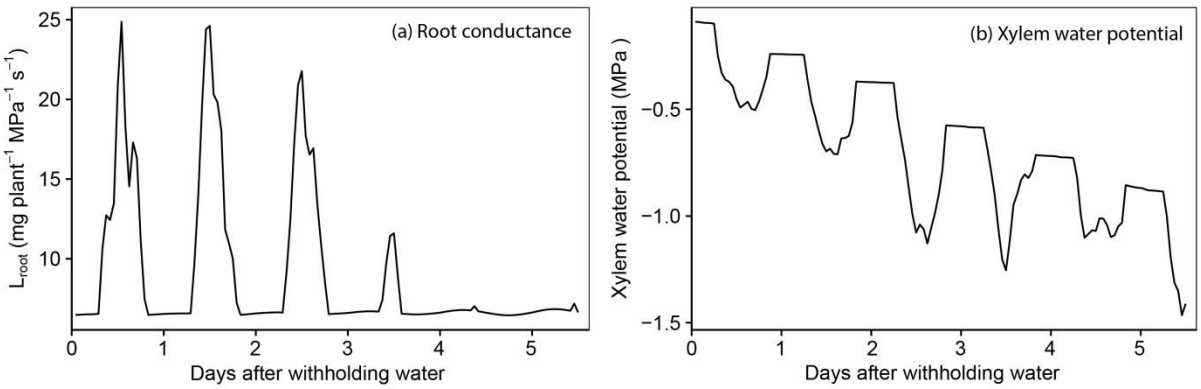

Fig. S8 The simulated diurnal changes of root conductance (a) and xylem water potential (b) within a soil drying cycle.

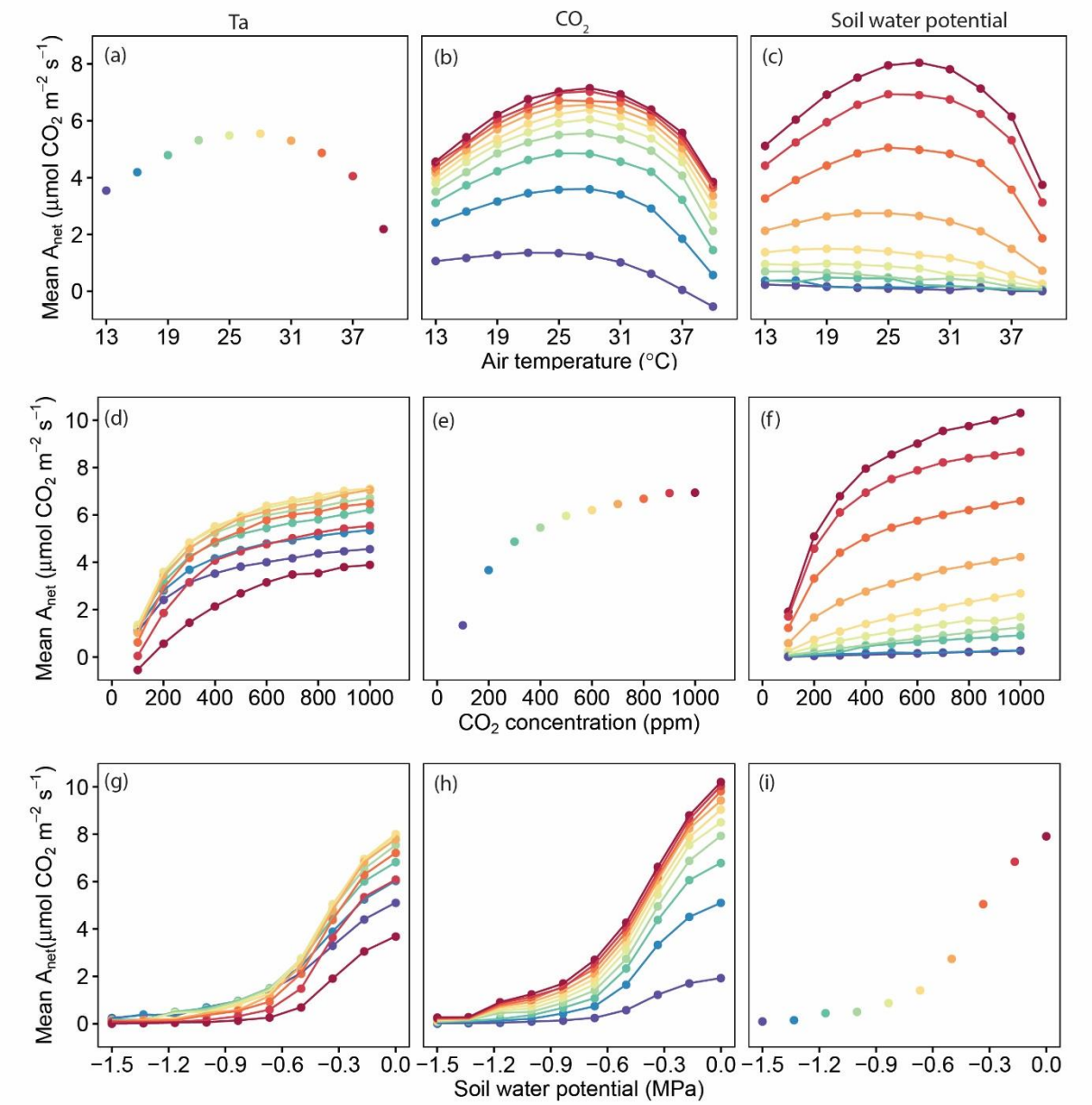

Fig. S9 The response of net photosynthesis to changes in temperature (column one and row one), CO_2 (column two and row two), and soil water potential (column three and row three). The figure is presented as an orthogonal square. The colours in column one represent different temperature as indicated in panel (a). The colours in column two represent different CO_2 as indicated in panel (e). The colours in column three represent different soil water potentials as indicated in panel (i). Note leaf temperature is approximately 3-5 ^{o}C higher than air temperature depending on the absorbed radiation and transpiration rate. The presented A_{net} is the mean A_{net} of all leaves of a plant.

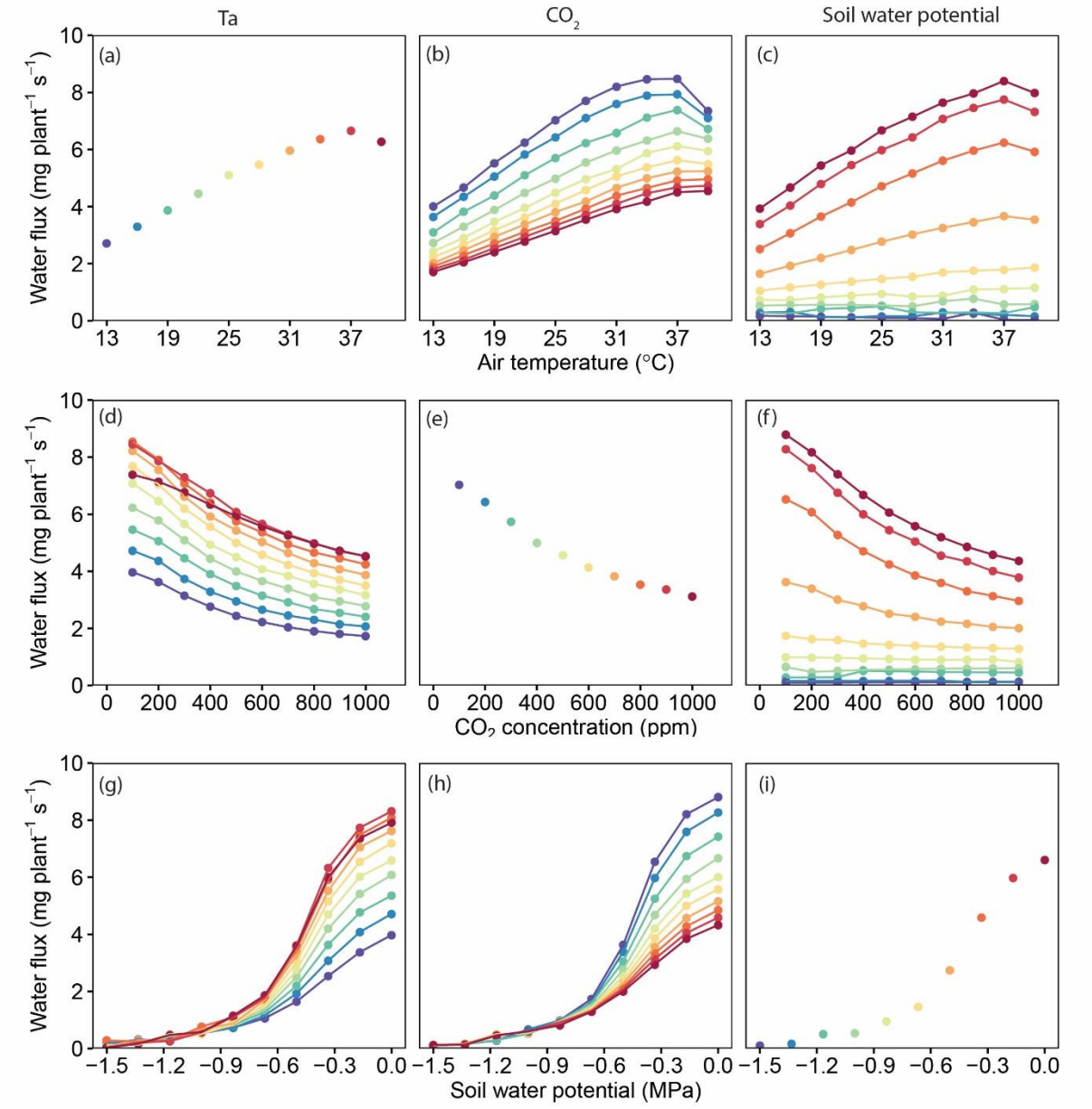

Fig. S10 The response of plant water flux to changes in temperature (column one and row one), CO_2 (column two and row two), and soil water potential (column three and row three). The colours in column one represent different temperature as indicated in panel (a). The colours in column two represent different CO_2 as indicated in panel (e). The colours in column three represent different soil water potentials as indicated in panel (i). Note leaf temperature is approximately 3-5 ^{o}C higher than air temperature depending on the absorbed radiation and transpiration rate.

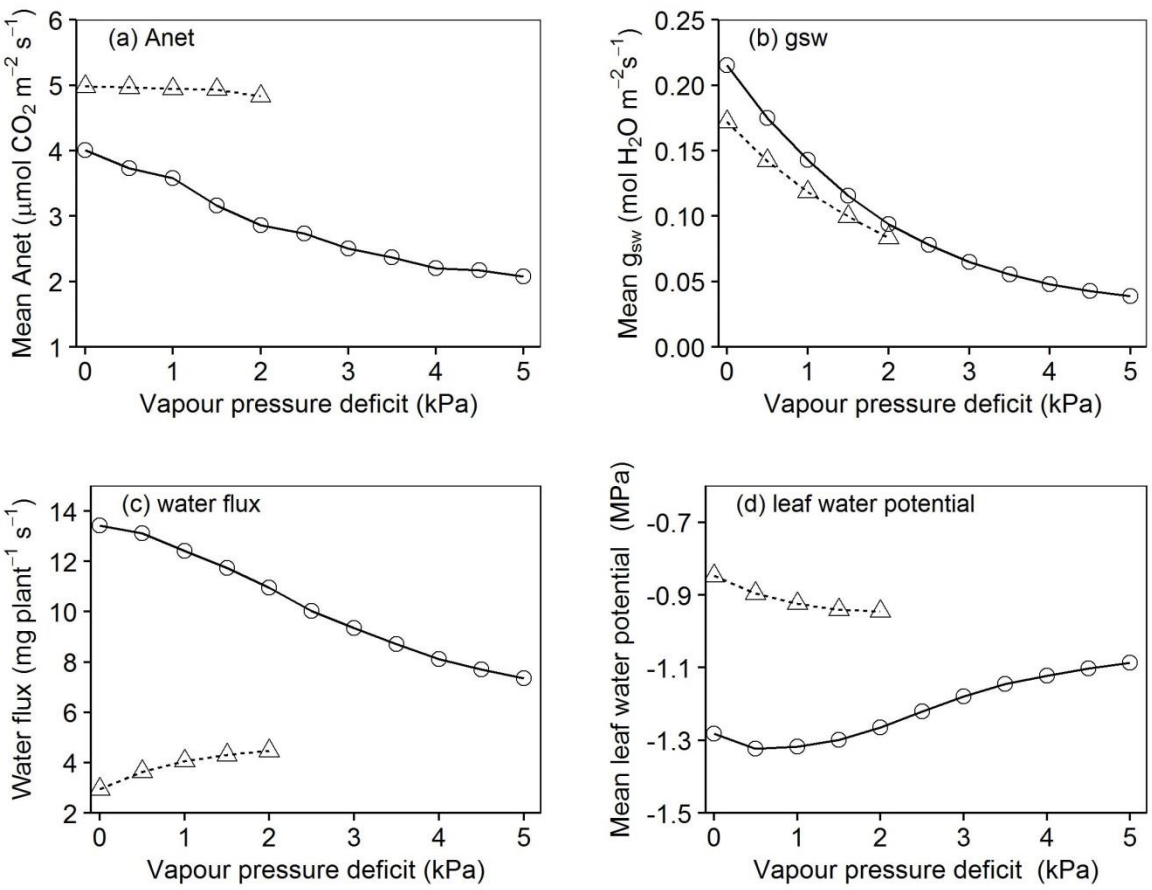

Fig. S11 The response of net photosynthesis (a), stomata conductance for water (b), whole plant water flux (c) and leaf water potential (d) to changes in vapour pressure deficit. Open circles and solid lines were simulations with high air temperature and high radiation (T_a equals to 35 ^oC and R_a equals to 4000 umol $m^{-2}s^{-1}$). Open triangles and dashed lines were simulations with low air temperature and radiation (T_a equals to 20 ^oC and R_a equals to 2000 umol $m^{-2}s^{-1}$). CO_2 was set to 400 ppm and ψ_{soil} was set to -0.3 MPa at both simulation scenarios. All simulations were made with nine plants, and only the middle plants were used in the calculation.

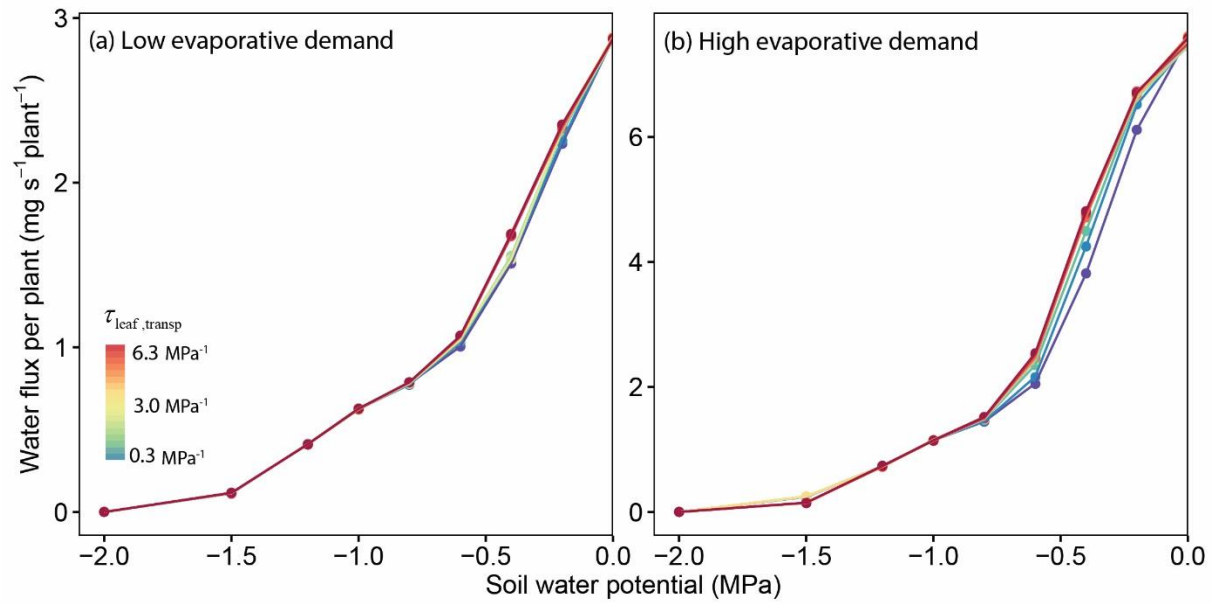

Fig. S13 The response of plant water flux at different soil water potentials to changes in to leaf conductance as induced by $\tau_{leaf,transp}$. Column one represents the low evaporative condition (2.4 mg plant^{-1} s^{-1}), and column two represents the high evaporative condition (6 mg plant^{-1} s^{-1}). Colour gradient from purple to red represents the increasing of the absolute value of the tested parameters, ranges from 10% to 210% of the default value (approximately the middle value in the legend). One extra simulation (dark red points and lines), 10 times of the default value was added for both $\tau_{g_s,ABA}$, and $\tau_{g_s,\psi_{leaf}}$.

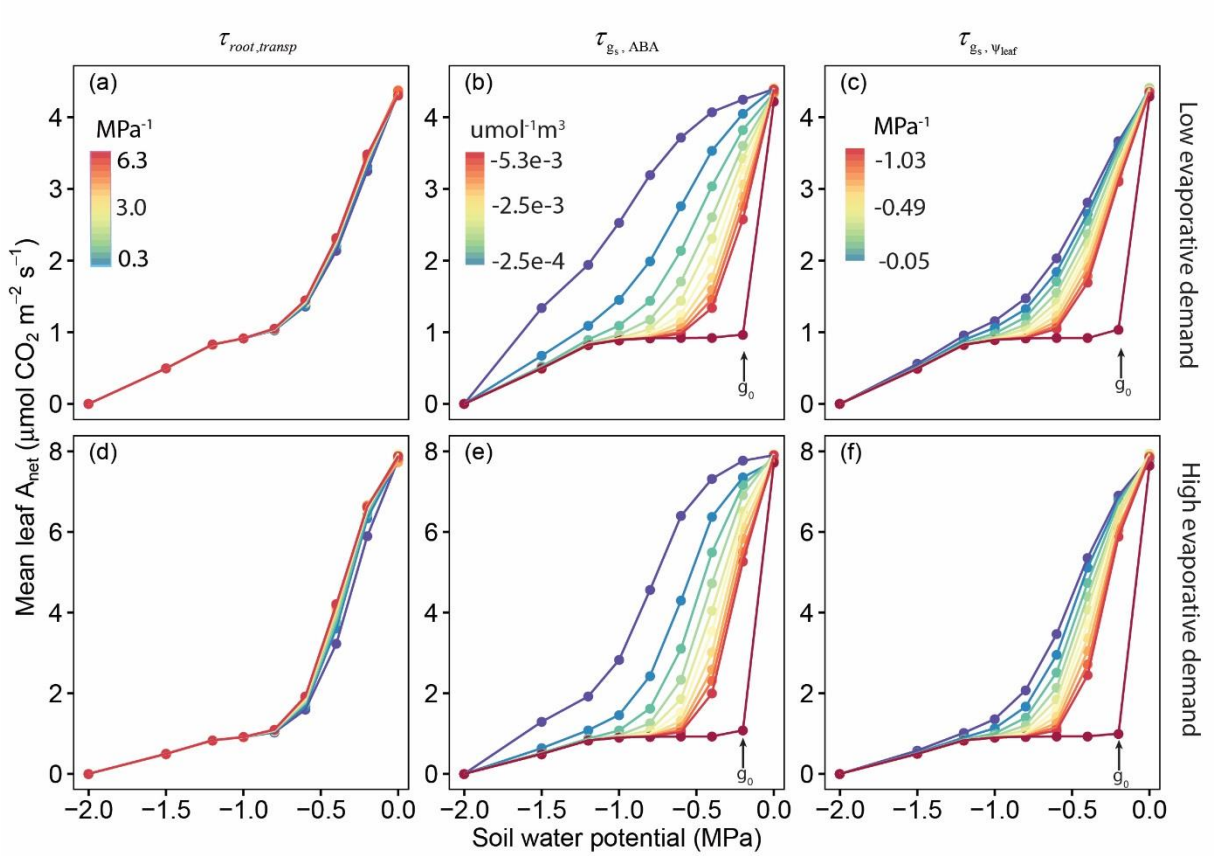

Fig. S14 The response of mean leaf net photosynthesis at different soil water potential to changes in potentials to changes in $\tau_{root,transp}$ (a, d), $\tau_{g_s,ABA}$ (b, e), and $\tau_{g_s,\psi_{leaf}}$ (c, f). Row one represents a low evaporative condition (2.4 mg plant^{-1} s^{-1}), and row two represents a high evaporative condition (6 mg plant^{-1} s^{-1}). Colour gradient from purple to red represents the increasing of the absolute value of the tested parameters, ranges from 10% to 210% of the default value (approximately the middle value in the legend). One extra simulation (dark red points and lines), 10 times of the default value was added for both $\tau_{g_s,ABA}$, and $\tau_{g_s,\psi_{leaf}}$.

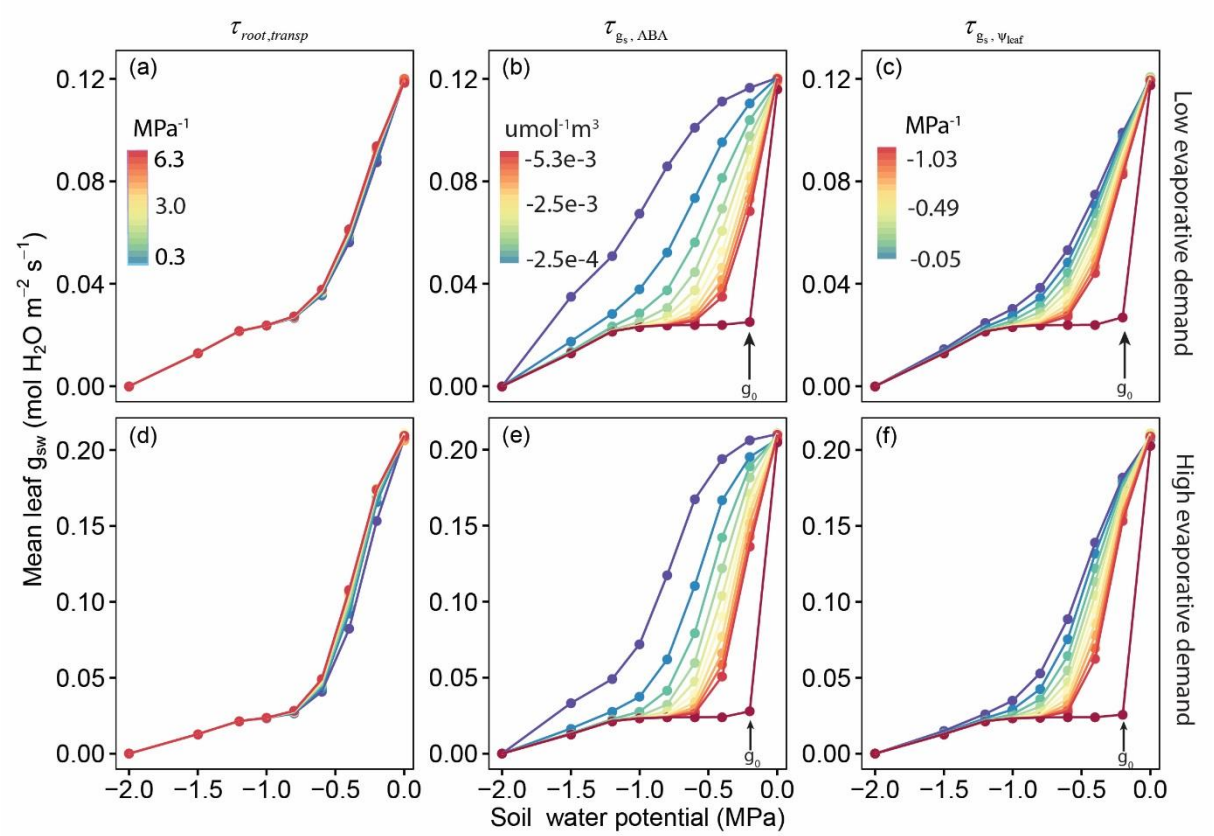

Fig. S15 The response of mean leaf stomata conductance at different soil water potentials to changes in $\tau_{root,transp}$ (a, d), $\tau_{g_s,ABA}$ (b, e), and $\tau_{g_s,\psi_{leaf}}$ (c, f). Row one represents a low evaporative condition (2.4 mg plant^{-1} s^{-1}), and row two represents a high evaporative condition (6 mg plant^{-1} s^{-1}). Colour gradient from purple to red represents the increasing of the absolute value of the tested parameters, ranges from 10% to 210% of the default value (median value in the legend). One extra simulation (dark red points and lines), 10 times of the default value was added for both $\tau_{g_s,ABA}$, and $\tau_{g_s,\psi_{leaf}}$.

.

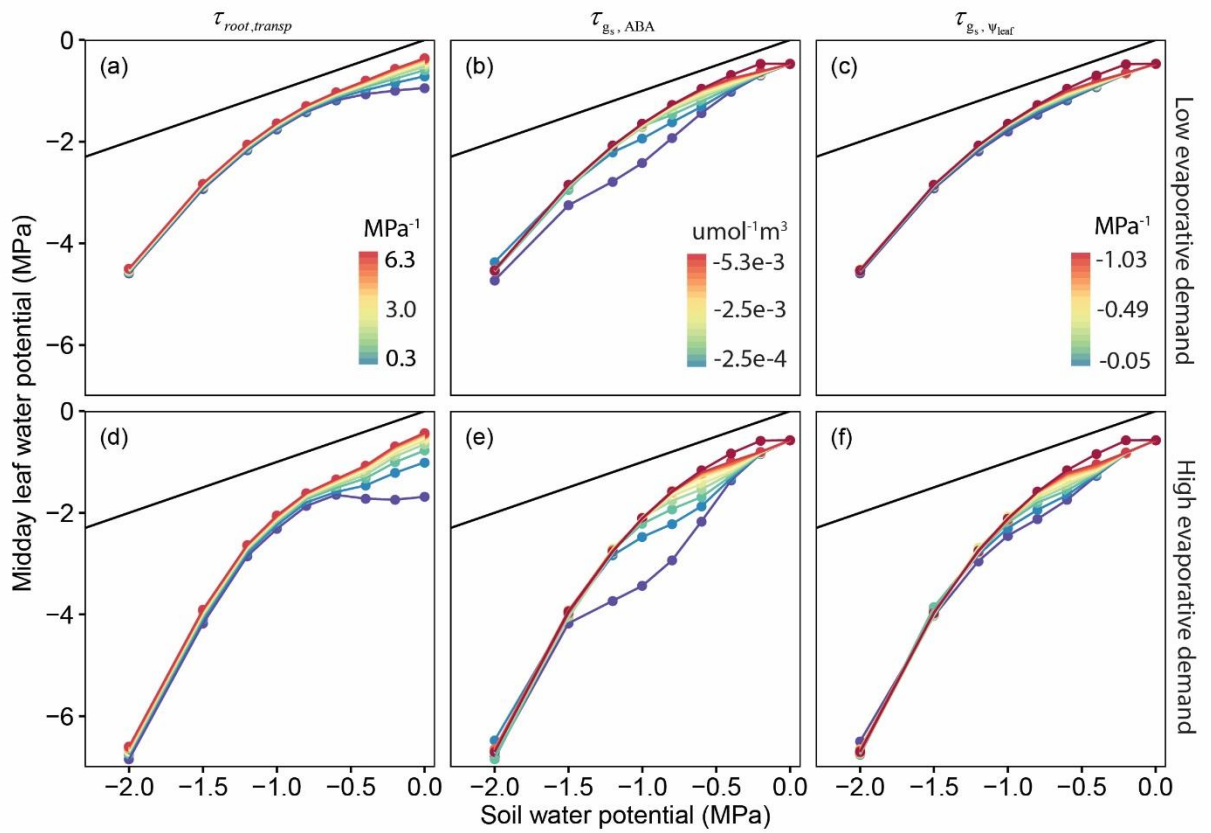

Fig. S16 The response of midday leaf water potential at different soil water potentials to changes in $\tau_{root,transp}$, $\tau_{g_s,ABA}$, and $\tau_{g_s,\psi_{leaf}}$ when removing the effect of f_{PLC} on g_0 (Eq. 1). Row one represents a low evaporative condition (2.4 mg plant^{-1} s^{-1}), and row two represents a high evaporative condition (6 mg plant^{-1} s^{-1}). Colour gradient from purple to red represents the increasing of the absolute value of the tested parameter, ranges from 10% to 210% of the default value. One extra simulation (dark red points and lines), 10 times of the default value was added for both $\tau_{g_s,ABA}$, and $\tau_{g_s,\psi_{leaf}}$. Black lines represent the 1:1 lines.

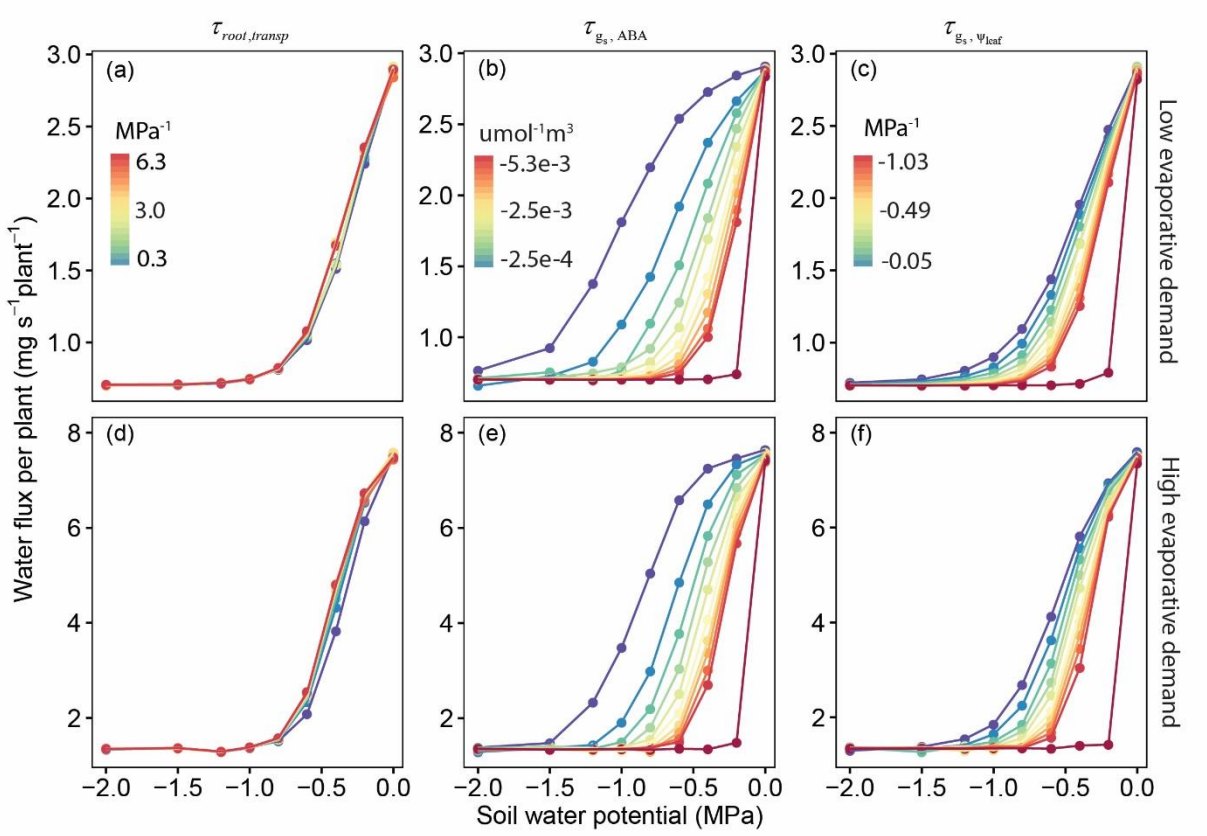

Fig. S17 The response of plant water flux at different soil water potentials to changes in $\tau_{root,transp}$ (a, d), $\tau_{g_s,ABA}$ (b, e), and $\tau_{g_s,\psi_{leaf}}$ (c, f) when removing the effect of f_{PLC} on g_0 (Eq. 1). Row one represents a low evaporative condition (2.4 mg plant^{-1} s^{-1}), and row two represents a high evaporative condition (6 mg plant^{-1} s^{-1}). Colour gradient from purple to red represents the increasing of the absolute value of the tested parameters, ranges from 10% to 210% of the default value (median value in the legend). One extra simulation (dark red points and lines), 10 times of the default value was added for both $\tau_{g_s,ABA}$, and $\tau_{g_s,\psi_{leaf}}$.

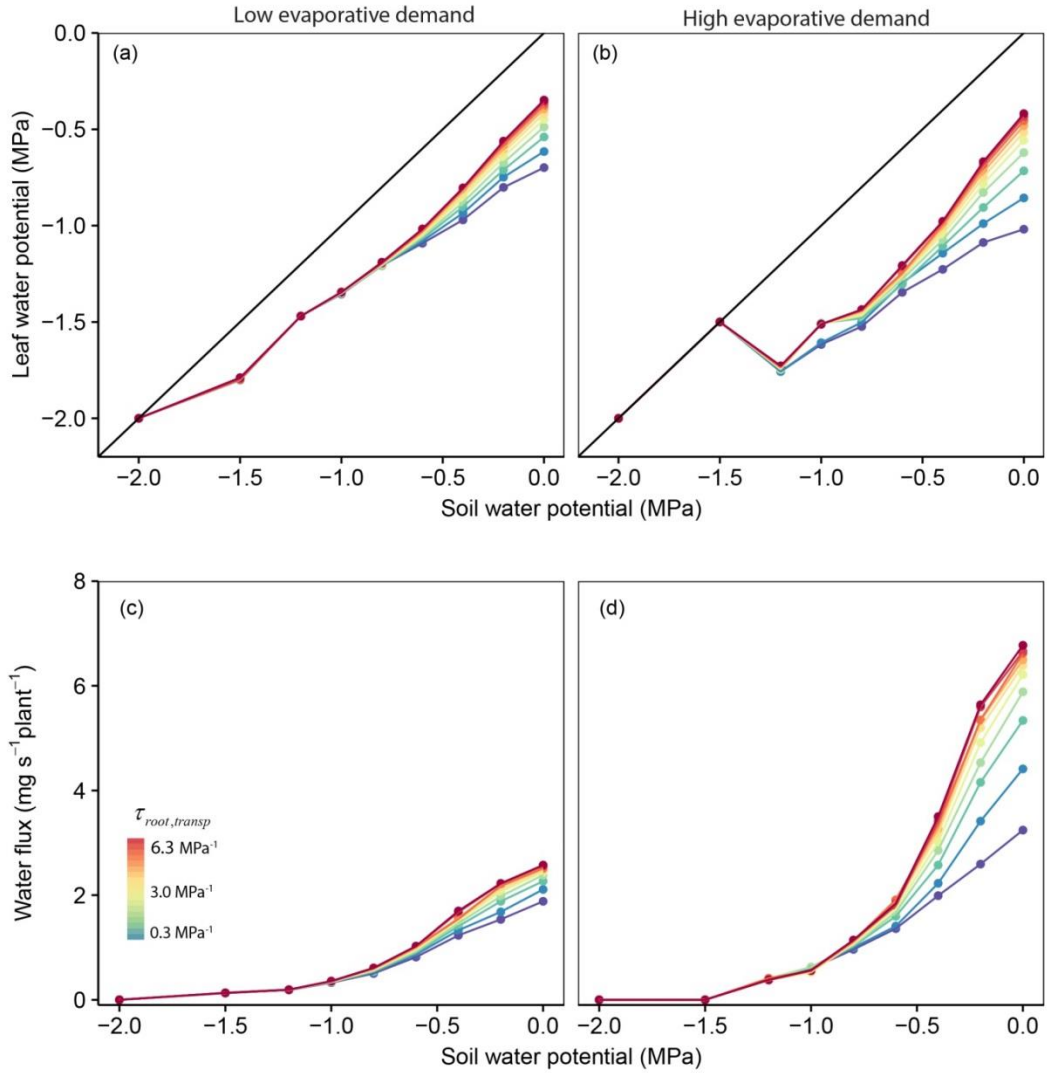

Fig. S18 The response of midday leaf water potential and plant water flux at different soil water potentials to changes in $\tau_{\text{root,transp}}$ without the effect of ABA. Column one represents the low evaporative condition (2.4 mg plant^{-1} s^{-1}), and column two represents the high evaporative condition (6 mg plant^{-1} s^{-1}). Colour gradient from purple to red represents the increasing of the absolute value of the tested parameter, ranges from 10% to 210% of the default value. During this simulation, stomata conductance was calculated by leaf water potential alone. As the exponential function ($g_{s,i} = g_0 \times (1 - f_{\text{PLC}}) + \alpha \exp(\tau_{g_{s,\psi_{\text{leaf},i}}} \psi_{\text{leaf},i})$) cannot fit our data well, so a logistic function ($g_{s,i} = g_0 \times (1 - f_{\text{PLC}}) + \frac{\alpha}{1 + \exp(a*(\psi_{\text{leaf,i}} - b))}$) was used for this simulation (a, b are fitted empirical coefficient).

Supporting Information data references

Evers JB, Vos J, Yin X, Romero P, van der Putten PEL, Struik PC. 2010. Simulation of wheat growth and development based on organ-level photosynthesis and assimilate allocation. *Journal of Experimental Botany* **61**: 2203–2216.

Greer DH, Weedon MM. 2012. Modelling photosynthetic responses to temperature of grapevine (*Vitis vinifera* cv. Semillon) leaves on vines grown in a hot climate. *Plant, Cell & Environment* **35**: 1050–1064.

Hochberg U, Albuquerque C, Rachmilevitch S, Cochard H, David-Schwartz R, Brodersen CR, McElrone A, Windt CW. 2016. Grapevine petioles are more sensitive to drought induced embolism than stems: evidence from in vivo MRI and microCT observations of hydraulic vulnerability segmentation. *Plant, Cell and Environment* **39**: 1886–1894.

Pantin F, Monnet F, Jannaud D, Costa JM, Renaud J, Muller B, Simonneau T, Genty B. 2013. The dual effect of abscisic acid on stomata. *New Phytologist* **197**: 65–72.

Prieto JA, Louarn G, Perez PeÑA J, Ojeda H, Simonneau T, Lebon E. 2012. A leaf gas exchange model that accounts for intra-canopy variability by considering leaf nitrogen content and local acclimation to radiation in grapevine (*Vitis vinifera L.*). *Plant, Cell & Environment* **35**: 1313–1328.

Tardieu F, Simonneau T, Parent B. 2015. Modelling the coordination of the controls of stomatal aperture, transpiration, leaf growth, and abscisic acid: update and extension of the Tardieu–Davies model. *Journal of Experimental Botany* **66**: 2227-2237.

Williams LE, Araujo FJ. 2002. Correlations among predawn leaf, midday leaf, and midday stem water potential and their correlations with other measures of soil and plant water status in Vitis vinifera. *Journal of the American Society for Horticultural Science* **127**: 448–454.

Yin X, Struik PC. 2009. C3 and C4 photosynthesis models: An overview from the perspective of crop modelling. *NJAS - Wageningen Journal of Life Sciences* **57**: 27–38.